J. Indian Inst. Sci.
A Multidisciplinary Reviews Journal
ISSN: 0970-4140 Coden-JIISAD

REVIEW ARTICLE

Strength–Ductility Synergy in High Entropy Alloys by Tuning the Thermo-Mechanical Process Parameters: A Comprehensive Review

Rushikesh Sabban[1], K. Dash[1], S. Suwas[2] and B. S. Murty[1,3]*

Abstract | The strength–ductility trade-off is an eminent factor in deciding the mechanical performance of a material with regard to specific applications. The strength–ductility synergy is generally inadequate in as-synthesized high entropy alloys (HEAs); however, it can be tailored owing to its tunable microstructure and phase stability. Thermo-mechanical processing (TMP) allows the microstructure to be tailored to achieve desired strength–ductility combination. The additional attribute is evolution of texture, which also significantly influences the mechanical properties. This review presents a critical insight into the role of TMP to achieve superior strength–ductility symbiosis at room temperature in single-phase (FCC, BCC) and multiphase HEA. The role of overall processing strategy of HEAs encompassing rolling and subsequent annealing in relation to the evolution of microstructure and texture in have been discussed. Recently practiced severe plastic deformation processes have also shown promise in improving the strength–ductility combination. The relevance of these processes in the processing of HEAs has also been analysed. At the end, futuristic approaches have been elaborated to enable efficient as well as hassle-free process towards achieving the proficiency of strength–ductility in HEAs.

Keywords: *High entropy alloy, Rolling, Thermo-mechanical processing, Strength–ductility synergy, Microstructure, Texture*

1 Introduction

High Entropy Alloys (HEA) are the class of alloys having minimum of five principal elements with a concentration of constituent elements between 5 and 35 at%[1–4]. The microstructure, properties, and performance of HEA are driven by four core effects, i.e., high configurational entropy[1,5], lattice distortion[3], sluggish diffusion[6], and cocktail effect[7]. Owing to these effects, HEA exhibit excellent tensile ductility, fracture toughness, corrosion resistance, and many other important properties of relevance[8–13]. The combination of desirable property attributes in HEAs makes these materials a perfect candidate for numerous applications, like in gas storage, in ion irradiation plants, and for biomedical implants[13–15]. The lower yield strength of many HEA, in as-synthesized condition, restricts their use in structural applications such as automobile sector[16]. Hence, enhancing the strength while maintaining ductility of HEA is a crucial factor to become potential structural material to compete with conventionally used materials in automobile and other sectors.

The HEA are synthesized conventionally through various routes such as melting and casting[17], powder metallurgy by mechanical alloying (MA) and sintering[18–21], surface deposition[22], etc. Techniques like additive manufacturing (AM)[23] and carbothermal shock synthesis (CTS)[24] have also been utilized widely in recent times. The HEA manufactured through these routes have inherent limitations including gas porosity,

[1] *Department of Metallurgical and Materials Engineering, Indian Institute of Technology Madras, Chennai 600036, India.*
[2] *Department of Materials Engineering, Indian Institute of Science, Bangalore 560012, India.*
[3] *Department of Materials Science and Metallurgical Engineering, Indian Institute of Technology Hyderabad, Kandi 502284, India.*
**bsm@iith.ac.in*

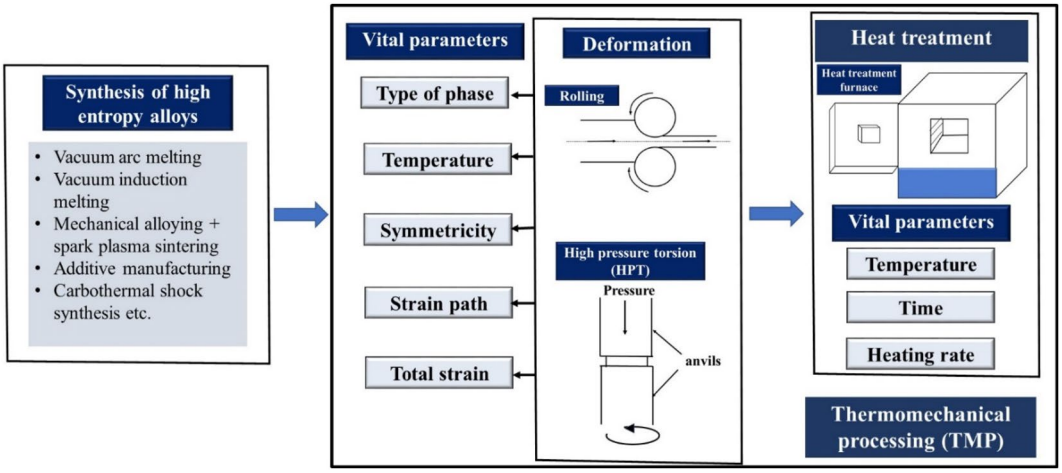

Figure 1: Schematic mentioning the various parameters of thermo-mechanical processing of high entropy alloys affecting the final mechanical properties.

shrinkage porosity, un-melted particles and detrimental microstructural features, etc.[25–27]. These defects in the specimens create inhomogeneous stress distribution which limit the optimum strength–ductility combination. The strength–ductility synergy is quantified as a product of strength and ductility (PSD in GPa × %) defined elsewhere[28]. Since the strength and ductility specifications for many room-temperature structural applications are critical, the synthesized HEA need to be engineered further to imbibe the desirable properties.

Thermo-mechanical processing (TMP) constitutes of a series of plastic deformation and thermal operations to tune the microstructure consequentially enhancing the strength–ductility synergy of as-synthesized components. The plastic deformation processes, like rolling, combined with a post-deformation annealing constitute the most commonly used sequence of a TMP schedule. A combination of rolling and heat treatment process (RHP) has been effectively utilized for aluminium, steel, and titanium alloys for enhancing room-temperature mechanical properties[29–31]. The rolling process, apart from changing the shape, is known to strengthen the as-cast or PM processed materials through various mechanisms such as dislocation strengthening, grain and twin boundary strengthening[32,33], etc. A subsequently optimized heat treatment facilitates the tailoring of the strength–ductility combination[34], leading to mechanical properties superior to as-cast or PM processed specimens.

The schematic Fig. 1 depicts three major modes of HEA processing along with key factors in individual stages. First step of HEA synthesis routes render characteristic microstructural features, e.g., type and fraction of phases, grain size, etc. All these parameters play a vital role in deciding post RHP properties[35,36]. During secondary processing, i.e., deformation through rolling or HPT, the working temperature along with recrystallization temperature governs the microstructural evolution. Rolling at various temperatures exhibits different strengthening mechanisms and hence influences the properties of HEA[37–39]. The rolling processes can be differentiated based on operating temperature which includes cryo-rolling (CR), room-temperature rolling (RTR), hot rolling above the recrystallization temperature (HR), and warm rolling (WR) (around average temperature of hot rolling and RTR). In addition to temperature, the parameters like amount of total strain, strain path, symmetricity of rolling (symmetric/asymmetric rolling), etc. also play an important role in ascertaining the final properties of an HEA[40–42]. During the heat treatment of the HEA, the annealing temperature primarily dictates microstructural evolution[43]. Additionally, the duration of annealing[44] and heating rate to achieve temperature of interest[45] also can be used to tune the strength–ductility synergy. Taken together, there are various parameters associated with different stages of TMP which decides the enhancement in tensile room-temperature mechanical properties of HEA.

There are a substantial number of journal papers on RHP of HEA starting from the year 2009. Figure 2 highlights the rapid increasing trends in number of publications in TMP starting from its inception. Review on evaluation

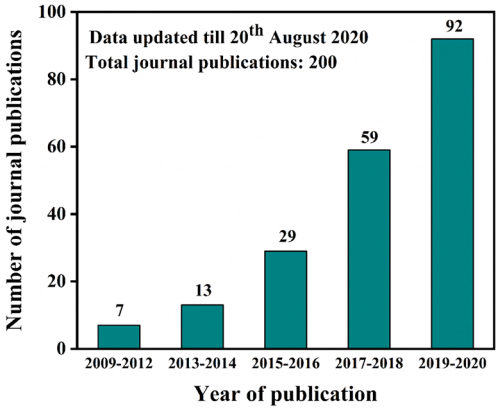

Figure 2: Graph indicating the number of journal publications on rolling annealing process of high entropy alloys.

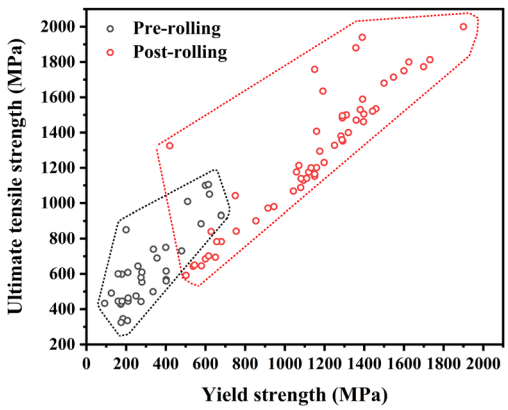

Figure 3: Ultimate tensile strength vs. yield strength graph implying the significant strengthening after rolling.

of mechanical properties of HEA through tensile and compressive behaviour has also been undertaken[46,47]. However, any of the reviews does not deal with the generic aspects of thermo-mechanical processing involving the rolling and annealing process. In summary, the focus of this review is to establish the role of variety of parameters in RHP process.

2 Strengthening HEA by Rolling

The rolling process in TMP has been effectively employed in the strengthening of as-synthesized HEA[48–53]. Figure 3 clearly indicates significant strengthening of HEA due to rolling. The compositions of HEA, rolling parameters, and percentage increase in the strength values after rolling have been given in Table 1. The primary strengthening mechanisms in HEA operative during rolling are associated with increased dislocation density[54], twin boundaries[37], kink bands[40], shear bands[55], grain refinement[56], transformation-induced plasticity[57,58], back stress hardening due to accumulation of dislocations[59–61], etc. In the following section, the tuning of various factors such as pre-rolling microstructural features, temperature of rolling, total strain, strain path, symmetricity, etc. and their corresponding strengthening mechanisms will be discussed.

2.1 Evolution of Deformed Microstructure Based on Phases

The various types of as-synthesized alloys with different phases can be classified as: (i) single-phase alloys: face-centered cubic (FCC)[50], body centered cubic (BCC)[40], B2 phase[62], etc.; (ii) multiphase alloys: FCC + BCC[63], FCC + hexagonal closed packed (HCP)[64], $L1_2$ + B2[65], etc. The deformation mechanisms active in these two types of alloys leading to strengthening will be elaborated in this section.

2.1.1 Single-Phase Alloys

During the initial stages, the single-phase FCC HEA undergo strengthening through dislocation activities leading to cell formation[66–68], deformation twins[69], microbands[70,71], shear bands due to heavy deformation[72,73], etc. At constant deformation temperature, the deformation of FCC HEA is primarily controlled by stacking fault energy (SFE)[74]. The nucleation of deformation twins is directly proportional to SFE[75,76]. Hence, the HEA with lower SFE exhibit deformation twinning as their deformation mechanism[77]. Additionally, with reduction in the SFE by tuning of composition of alloy, the deformation twin thickness can also be reduced[76]. This reduction of twin thickness will provide higher strengthening in FCC HEA[78]. In contrast, the increase in SFE (lowering the distance between Shockley partials) leads to easier cross-slip. Hence, at higher SFE values, microband formation was found to be dominant mechanism for deformation[79]. The deformation mechanism changes from twinning to microband formation with increasing nitrogen content[70]. The SFE increases by alloying elements like nitrogen leading to change in the deformation mechanism[80]. To sum up, in the initial and intermediate stages of deformation, the microstructural evolution and strengthening in FCC HEA is influenced by SFE.

Table 1: Strengthening of as-synthesized high entropy alloys after rolling.

Composition of HEA	No. of phases	Structure of phases present	Rolling details (rolling temperature/reduction in thickness)	Yield strength (MPa)	Ultimate tensile strength (MPa)	Increase in yield strength (%)		Increase in ultimate tensile strength (%)		Reference
						Before rolling	After rolling	Before rolling	After rolling	
$Al_{0.1}CoCrFeNi$	Single	FCC	RTR/ 75%	200	1198	850	1230	499	45	137
$Al_{0.25}CoCrFeNi$	Single	FCC	RTR/ 90%	126	1292	491	1481	925	202	48
$Al_{0.25}CoCrFeNi$	Single	FCC	RTR / 60%	173	1080	428	1088	524	154	50
$Al_{0.25}CoCrFeNi$	Single	FCC	RTR / 60%	260	1150	644	1160	342	80	50
$Al_{0.25}CoCrFe_{1.25}Ni_{1.25}$	Single	FCC	RTR/ 80%	92	616	433	702	570	62	39
$Al_{0.3}FeCoCrNiMn$	Single	FCC	RTR / 96%	275	1459	443	1534	431	246	51
$Al_{0.3}CoCrFeNi$	Single	FCC	RTR/ 70%	207	420	335	1325	103	296	41
$Al_{0.3}CoCrFeNi$	Single	FCC	RTR/ 90%	175	1283	325	1380	633	325	169
$Al_{0.45}CoCrFeNi$	Single	FCC	RTR / 70%	209	1100	608	1137	426	87	52
$Al_{0.5}CoCrFeNi$	Dual	FCC + BCC	RTR/ 50%	402	1396	568	1461	247	157	43
$Al_{0.5}CoCrFeNi$	Dual	FCC + BCC	RTR/ 20%	402	755	616	842	88	37	21
$Al_{0.5}CrCuFeNi_2$	Single	FCC	RTR/ 50%	402	1132	560	1200	182	114	154
$AlCoCrFeNi_{2.1}$	Dual	$L1_2$ + B2	Cryo-rolling/ 45%	600	1600	1100	1750	167	59	55
$AlCoCrFeNi_{2.1}$	Dual	$L1_2$ + B2	Cryo-rolling + warm rolling/ 90%	600	1900	1100	2000	217	82	55
$AlCoCrFeNi_{2.1}$	Dual	$L1_2$ + B2	Cryo-rolling/ 90%	615	1699	1105	1773	176	60	65
$AlCoCrFeNi_{2.1}$	Dual	$L1_2$ + B2	RTR/ 90%	620	1625	1050	1800	162	71	168
$AlCoCrFeNi_{2.1}$	Dual	$L1_2$ + B2	Warm rolling/ 90%	510	1390	1009	1940	173	92	41
$AlCoCrFeNi_{2.1}$	Dual	$L1_2$ + B2	RTR/ 90%	615	1731	1105	1813	181	64	22
$Al_{3.4}C_{0.7}CoCrFeNiMn$	Single	FCC	RTR/ 80%	210	1310	445	1500	524	237	111
CoCrFeMnNi	Single	FCC	RTR / 60%	184	854	346	901	364	160	70
1 at% N- CoCrFeMnNi	Single	FCC	RTR / 60%	280	1043	554	1068	273	93	70
CrMnFeCoNi	Single	FCC	RTR / 90%	210	1150	463	1152	448	149	140
CrMnFeCoNi	Single	FCC	RTR/ 50%	210	1250	463	1327	495	187	140

Table 1: (continued)

Composition of HEA	No. of phases	Structure of phases present	Rolling details (rolling temperature/reduction in thickness)	Yield strength (MPa)	Ultimate tensile strength (MPa)	Increase in yield strength (%)		Increase in ultimate tensile strength (%)		Reference
						Before rolling	After rolling	Before rolling	After rolling	
0.69 at% C-CoCrFeNiMn	Single	FCC	RTR / 80%	275	1310	580	1500	376	159	136
FeCoCrNiMn-1 at % C	Single	FCC	RTR/ 80%	400	1360	750	1470	240	96	79
CoCrFeNiMn	Single	FCC	RTR/ 80%	160	1120	445	1175	600	164	42
FeCrCoMnNi	Single	FCC	RTR / 90%	210	1150	447	1164	448	160	140
$CoCrFeNiMo_{0.2}$	Single	FCC	RTR/ 80%	280	1392	610	1589	397	160	170
$CoCrFeNiNb_{0.1}$	Single	FCC	RTR/ 25%	250	650	475	694	160	46	92
$CoCrFeNi2.1Nb_{0.2}$	Dual	FCC + Laves	Cryo-rolling/ 90%	178	1150	598	1758	546	194	49
CoCrFeMnNi	Single	FCC	RTR/ 80%	356	1292	690	1352	263	96	132
$CoCrFeNiNb_{0.1}$	Single	FCC	Cryo-rolling/ 25%	250	600	475	685	140	44	92
CoCrFeNiMn	Single	FCC	RTR/ 80%	180	1059	445	1176	488	164	37
CoCrFeNiMn	Single	FCC	Cryo-rolling/ 80%	180	1398	445	1504	677	238	37
FeCrCuMnNi	Single	FCC	Cryo-rolling/ 85%	336	1176	499	1294	250	159	108
$Fe_{28.2}Ni_{18.8}Mn_{32.9}Al_{14.1}Cr_6$	Single	FCC	RTR/ 65%	679	1442	931	1521	112	63	37
$CoCrFeNi_{2.1}Nb_{0.2}$	Dual	FCC + Laves	RTR/90%	160	1380	600	1530	763	155	60
$CoCrFeNi_{2.1}Nb_{0.4}$	Dual	FCC + Laves	RTR/90%	480	1500	730	1680	213	130	60

In BCC HEA, the deformation is driven by mechanisms such as increase in dislocation density[40], kink bands[81], deformation bands[82,83], microbands[84], shear bands[40], etc. The misorientation of boundaries was found to be related to kink bands[40,81,85] after rolling which was lower compared to the misorientation of twin boundary in BCC HEA[40,81,86]. Along with BCC alloys, the partially ordered single-phase B2 also deforms primarily by dislocation microbands formation[62]. The formation of microbands in B2 has been attributed to the preference of deformation via planar slip over other mechanisms[71], wherein the leading Shockley partially destroys the barrier for ordering of B2 phase making it easy for trailing Shockley partial to continue planar slip leading to formation of microbands[62,87]. At larger plastic strains, the shear band formation is the dominant mechanism for most of the HEAs irrespective of initial phase[40,72]. The shear band formation represents plastic instability[88] and occurs irrespective of crystallography of sample at sufficiently larger rolling deformation[89]. Taken together, there are variations in deformation mechanisms possible in single phases based on type of phase and SFE.

2.2 Multiphase Alloys

The deformation mechanisms of multiphase alloys include most of the mechanisms applicable to single-phase alloys, such as dislocation cell formation[43,60], deformation twinning[73,90], shear banding[65,73], etc. In addition, the multiphase alloys have additional strengthening mechanisms such as back stress strengthening due to accumulation of dislocations at phase boundaries[59–61], strain-induced martensitic transformation[73,90], etc. The major strain partitions to soft FCC phase compared to hard phases like carbides, ordered phase B2, etc. For maintaining continuity, the geometrically necessary dislocations (GNDs) participate in the deformation, which provides additional strengthening in dual-phase alloys compared to single-phase alloys[59]. The mechanism of strain-induced FCC-to-HCP martensite transformation in the dual-phase alloy containing FCC and thermally stabilized HCP phase has also been reported[64]. The stacking fault generated in the initial stages of deformation in FCC phase acts as nuclei for transformation of FCC phase to HCP martensite[91]. Hence, in general, the strengthening effect is higher in dual-phase HEA compared to single-phase HEA.

2.3 Development of Microstructure at Different Rolling Temperatures

As described in previous section, the active strengthening mechanisms in HEA are dislocation activity[50], microbands[71], stacking fault (SF)[92], deformation twinning[70], shear bands[93], etc. depending on pre-rolling phases and SFE. The selection and evolution of any of the above-mentioned mechanisms, however, depends on the rolling temperature[37]. During cryo-rolling (CR) and room-temperature rolling (RTR), the evolution of microstructure is governed by dislocation activity and twinning depending on SFE of HEA. The SFE of the conventional alloys and HEA is directly proportional to temperature[92,94]. Hence, during CR and RTR, the microstructural evolution will change according to SFE. However, at higher temperature regime (near or above the recrystallization temperature of alloy), the microstructural changes will get affected by thermal activation. The effect of rolling temperature at elevated temperatures on properties can be explained through change in Zener–Hollomon (Z–H) parameter[95]. At constant strain rate, lowering the rolling temperature increases the Z–H parameter and the strength thereof. In this section, the difference in mechanisms of strengthening and their effect on properties after rolling at different temperatures will be discussed.

2.3.1 Deformation at Room Temperature and Cryogenic Temperature

The difference in the mechanical properties with change in the rolling temperature in the temperature regime spanning from room temperature to cryogenic temperature is shown in Fig. 4. Figure 4a describes the difference in hardening at two rolling temperatures of $CoCrFeNiMo_{0.15}$ HEA[71] and Fig. 4b highlights the effect of rolling temperature on strengthening in CoCrFeNiMn alloy[37]. The cryo-rolled (CR) specimens exhibited more strengthening than room-temperature rolled (RTR) specimens. The difference between RTR and CR is that the microstructural evolution kinetics is faster in the latter[37,71,92,96]. The initial stages of deformation in RTR are dominated by dislocation activity and SFs, and with increasing strain, the deformation twins become dominant. The SFE of the studied alloy is low, and hence, deformation twining is favorable over microbands at room temperature[75]. Compared to RTR specimens the activation of deformation

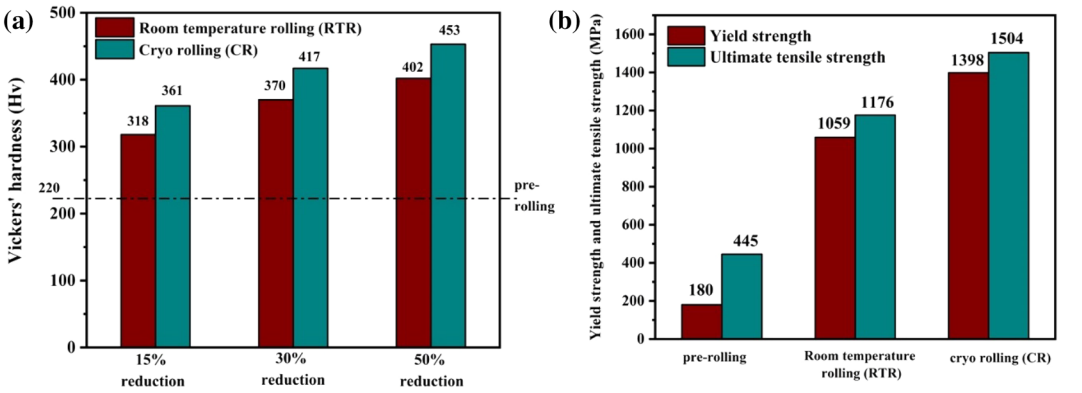

Figure 4: The different amount of strengthening achieved through rolling at cryo and room temperature in high entropy alloys: **a** $CoCrFeNiMo_{0.15}$[71]; **b** CoCrFeNiMn[37].

twinning for CR specimens happened at earlier stages. This is explained with the fact that the SFE at liquid nitrogen temperature is further less compared to SFE at room temperature[92]. With increasing strain in CR, the multiple twin systems get activated and distortion of nanotwins occurs later. The shear bands were also found post CR after imparting high strain[37,71,96]. The enhanced dislocation density was also observed in the conventional FCC alloys after deforming at cryo-temperature in comparison with room temperature[97]. The deformation-driven FCC-to-HCP transformation-induced plasticity (TRIP) was observed after CR. The SFs present in the initial stages acted as nucleating sites for FCC-to-HCP transformation[64]. The texture after CR and RTR was brass-type texture which is typical for low SFE material[93]. Hence, there is little role of texture in additional strengthening after CR than RTR. Hence, the HEA exhibits the enhanced strengthening at cryo-temperature compared to room temperature (Fig. 4a, b) due to higher dislocation density, intersection of twins from non-parallel systems, TRIP, and more shear banding.

2.4 Warm and Hot Deformation

The influence of rolling in high-temperature regime at intermediate as well as at high temperatures, namely warm rolling (WR)[98] and hot rolling[99–102], has been investigated for HEAs. In general, hot working refers to rolling at temperatures above the recrystallization temperature[103], while warm rolling is performed at intermediate temperatures of cold and hot rolling[55]. For the HEAs that are less workable, hot working is preferred[35]. Another associated attribute of deformation at high temperature is associate control of microstructures[55,100]. The hot rolling of HEAs involves dynamic recovery, dynamic recrystallization, grain growth, etc. as other micro-mechanisms like phase evolution and transformation depending on rolling temperature[100,104]. Mostly recovery and partial recrystallization is prevalent in the FCC HEA rolled at temperatures below recrystallization temperature of HEA[100]. This recovery-to-recrystallization ratio is strongly dependent on temperature and SFE of the material. Recovery is dominant at lower rolling temperatures and in high SFE alloys, while at higher rolling temperatures and for low SFE alloys, recrystallization is more prevalent[105]. For HEAs, increased degree of recrystallization is observed at higher rolling temperatures[100]. For much higher rolling temperatures, grain growth has also been observed[100] due to increased mobility of grain boundary at higher temperature[105]. The microstructural transformation through any of these routes led to specific strength–ductility synergy in the HEA.

The deformation mechanisms during the warm rolling of $AlCoCrFeNi_{2.1}$ eutectic HEA were found to be function of rolling temperature[55]. The shear banding and disordering of $L1_2$ phase was influenced by rolling temperature. In the dual-phase (FCC + BCC) $Al_{0.5}CoCrFeMn$ HEA, the FCC phase underwent deformation, while the harder BCC phase underwent grain fragmentation instead of deformation[35]. Another influence of temperature was noticed in terms of propensity of twinning. Twinning was reported to be suppressed with increase in temperature in warm working regime due to increase in SFE in the HEAs that exhibit twinning induced plasticity (TWIP)[106].

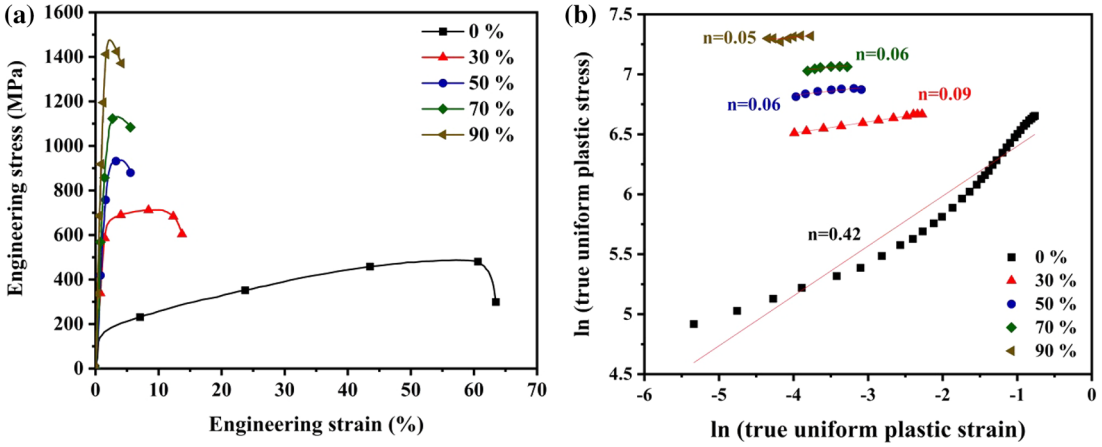

Figure 5: **a** The engineering stress–strain curve of $Al_{0.25}CoCrFeNi$ high entropy alloy before and after various reduction in thickness[48]; **b** the corresponding ln (true uniform plastic stress) vs. ln (true uniform plastic strain) plot for strain hardening analysis with values of strain hardening exponent(n) mentioned.

In general, the strength–ductility combination has been tailored by a combination of deformation in multiple temperature domains, for example, a combination of cryo-rolling and warm rolling. This combination results in generation of heterogeneous microstructure to enhance the strength–ductility synergy[53]. Such a processing is sometimes referred to as hybrid processing or hybrid rolling. To summarize, a broad range of micro-mechanisms act to play, depending on the working temperature. Hence, by varying the rolling temperature, hence by tailoring the microstructure optimally, the strength–ductility combination can be fine-tuned.

3 Total Plastic Strain

The evolution of microstructure in various HEA with increasing rolling reductions (plastic strains) and its effect on mechanical properties thereof has been evaluated extensively[107–109]. The evolution of strength after cold rolling in FCC HEA $Al_{0.25}CoCrFeNi$ with increasing total plastic strain Fig. 5[48]. The increase in % thickness reduction led to increase in strength at the cost of ductility (Fig. 5a). The strain hardening analysis has been carried out on results presented in Fig. 5a. The strain hardening regime of stress–strain curve (between yield strength and ultimate tensile strength) was considered for the calculations of specimens rolled to different reductions. The Hollomon analysis plot (ln (true uniform plastic stress) vs. ln (true uniform plastic strain)) after various rolling reductions is presented in Fig. 5b. The details of the Hollomon calculation can be found elsewhere[110]. The slope of the curve after applying linear regression ($R^2 > 0.8$) is the strain hardening exponent (n). Figure 5b highlights the decrease in 'n' (early necking) after increasing the rolling reduction. Similar behavior was observed for some HEA[111,112] and conventional aluminium alloys[110]. The decrease in strain hardening capacity in $Al_{0.25}CoCrFeNi$ HEA with increasing rolling reduction can be explained based on deformation mechanisms. The mechanisms of deformation in various phases are different at different temperatures, and dislocation activity and cell formation are the dominant mechanism of deformation in the initial stages[43,60]. As the deformation proceeds, the multiplication of dislocations and sub-grain size refinement take place which makes it difficult for further strain hardening and non-uniform deformation leads to necking[110]. Taken together, the strength evolution as a function of plastic strain has been observed and increased strengthening can be achieved with increasing plastic strain.

4 Tuning the Strain Path

The effect of varying strain path during rolling on microstructure evolution and final properties in the conventional alloys containing different phases has been well studied[113–115]. The elongated grain structure is developed by virtue of unidirectional rolling (UDR), whereas the lamellar structure fragmentation occurs by cross rolling. There are a few reports on difference in microstructure due to strain path change in HEA[41,117,118]. The variation in deformation microstructure gives rise to difference in the mechanical properties post-annealing. In the case of the HEA

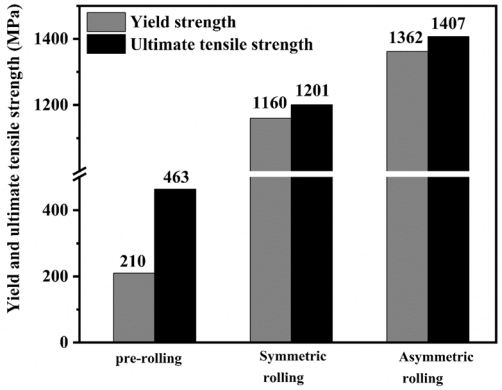

Figure 6: The difference in strengthening with symmetric and asymmetric rolling at room temperature in CoCrFeMnNi alloy[42].

$AlCoCrFeNi_{2.1}$, the UDR sample resulted in heterogeneous microstructure with lamellar and recrystallized grains in contrast to cross-rolled specimens which exhibited duplex recrystallized grains. Subgrains are well developed in UDR specimen, whereas it gets distorted during cross rolling. The destabilization of dislocation structure during cross rolling is also reported in the case of cold rolling of CoCrFeMnNi FCC alloy[117]. This destabilization effect has also been reported in the conventional FCC alloys[114,119], and the distortion in development of misorientation provides lesser nucleating sites for recrystallization leading to coarse grain size in cross-rolled specimens in comparison to UDR[117]. The difference in the grain size affects the strength–ductility synergy[120]. The increase in the volume fraction of intersecting twins in low SFE HEA after cross rolling and intermittent annealing due to destabilization of substructure has also been reported[118]. Therefore, it is clear that changing the strain path during rolling could enable the microstructure and strength–ductility combination to be tuned.

5 Symmetricity of Rolling

The symmetricity of rolling can be varied by varying the (a) diameter of the rolls, (b) friction conditions at the roll and sample surface, and (c) the speed of the roll[121,122]. Along with plain strain compressive stress (as in conventional rolling), asymmetric rolling imparts additional shear stress during deformation[122]. The equivalent strains in asymmetric rolling were also found to be slightly higher compared to the conventional rolling[123]. Researchers have utilized asymmetric rolling for refining the microstructure and enhancing the mechanical properties of conventional aluminium, magnesium alloys[123–125], etc. The process of asymmetric rolling (ASR) at room temperature using different roll speeds (speed ratio 1.5) for FCC CoCrFeMnNi alloy was also performed[42]. Asymmetrical rolling strengthened the HEA by 96% more in comparison with symmetric rolling (SR) (Fig. 6). As discussed earlier, the deformation mechanisms dominant in FCC HEA are dislocation cell formation, deformation twinning, shear bands, etc.[43,65,90]. The CoCrFeMnNi alloy exhibited a higher number of dislocation cell formation in ASR compared with SR specimens. The asymmetrically rolled FCC metals like aluminium exhibited higher percentage of low-angle grain boundaries (LAGBs) converted to high-angle grain boundaries (HAGBs) due to higher dislocation activity. This conversion was promoted by additional shear stress[123]. In addition to dislocation activity, SR specimens showed parallel set of deformation twins in contrast to intersecting twins in ASR specimens. These intersecting twins exhibit additional hardening in ASR specimens[126]. Higher volume fraction of shear bands formation was seen in ASR as compared to conventionally rolled specimens. The complex strain distribution in ASR is reported to be the plausible reason for higher fraction of intersecting twins and shear bands[124,126]. Owing to the above-mentioned discussion, ASR displays additional strengthening in comparison with SR specimens. Similar kind of additional strengthening in FCC HEA has been reported with different roll speeds[127]. The dislocation density is found to be twice in ASR specimens compared to SR. Asymmetric rolling is proven to be effective way to attain the additional strengthening compared to symmetric rolling for HEA.

5.1 Deformation Texture

The generation of texture during TMP of HEA significantly influences the strength of the material. Orientation of grains in HEA post TMP is decided by the strain path, working temperature, and the recrystallization parameters. Texture evolution in HEA post-deformation in HEA is discussed here based on phases present in the alloy. Table. 2 shows the deformation and annealing texture components of common HEA.

HEA like Cantor alloy contain typical rolling components post-room-temperature rolling (RTR) such as Bs, Cu, cube, and S components. The S component strengthens up to 80% RTR reduction, beyond which it decreases[129]. The brass component strengthens beyond 80% and keeps on increasing till 90%

Table 2: Deformation and annealing texture components of HEA.

Rolling conditions	Composition	Phase	Deformation texture	Recrystallization texture	Recrystallization temperature (°C)	Ref. no
RTR	CoFeNi	FCC	Bs, S	Cube	700–1000	38
	CoCrFeNi		S, Bs	Random		
	CoCrFeMnNi		Bs	Random		
RTR	CoCrFeMnNi	FCC	Bs, Cu, cube, S	K{142}<2 $\bar{1}$ 1>, M{13 6 25}<20 15 $\bar{1}$4>	650–1000	129
WR	AlFeCrCoNi$_{2.1}$	$L1_2$	Bs, G, G/B	Bs, G, G/B	800–1200	130
		B2	{112}<110>	{112}<110>	800	
				{111}<110>	1200	
CR	AlFeCrCoNi$_{2.1}$	L12	Bs, Goss, Rt-Goss	Bs, Goss, Rt-Goss	800–1200	49
		B2	{001}<110>	ND fibre		
RTR	HfZrTiTaNb	BCC	ND, RD fibre	{111}<110>	1400	131

reduction. Slip planes at low RTR reduction and fine lamellae with deformation bands co-existing at high RTR reduction are responsible for the texture development. The Goss and Bs components show up in the FCC phase of FeCrCuMnNi in 90% RTR alloy[109]. Twins present in the Cantor alloy promote the transition of Cu to brass type of texture to during RTR[126]. $Al_{0.5}$CoCrFeNi HEA shows {110}<112> and {111}<110> components on RTR possessing FCC with trace BCC phase, which on recrystallization become weak[43]. Cryo-rolling of Cantor alloy shows a similar texture as after cold rolling[93]. Multistage cross cold rolling of Cantor alloy shows stronger Bs component than unidirectional rolled specimen[117].

The $L1_2$ phase in the eutectic HEA AlFeCrCoNi$_{2.1}$ possesses Bs type of texture post-warm rolling along with α-fibre (Goss, Bs, G/B); whereas the B2 phase shows {112}<110> type of texture along with RD||110 and ND||111 fibres post-warm rolling[130]. Different strain paths imparted at cryo-temperature on EHEA generate Bs along with Goss, Rt-Goss in $L1_2$ phase, and {001}<110> in B2 phase after multistep cross rolling[41]. HfZrTiTaNb HEA with BCC phase, when cold rolled, exhibits strong ND fibre (ND//<111>), and RD fibre (RD//<110>) along with cube and Rt-cube components[131].

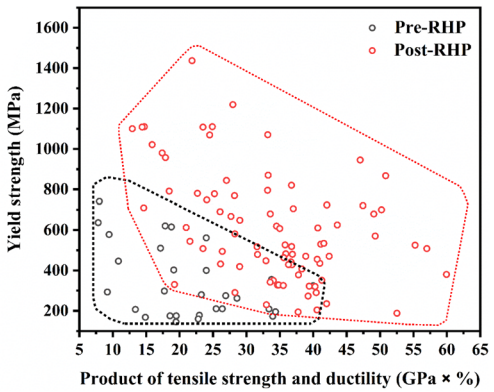

Figure 7: Yield strength vs. product of ultimate tensile strength and ductility graph highlighting the enhancement in strength–ductility synergy through RHP of high entropy.

6 Post-rolling Heat Treatments: Annealing

Rolling leads to strengthening of HEAs, compromising on the ductility factor[132,133]. The strength–ductility combination has been optimized by designing different heat treatment regimens post-rolling, which is plotted and highlighted in Fig. 7[128,134,135]. The composition of the alloys with respective RHP and properties are presented in Table 3. The quantification of strength–ductility synergy which is realised by the parameter PSD (GPa × %) displays that RHP has significantly enhanced the strength–ductility combination of as-synthesized HEA (Table 3). This improvement is dependent on the cascade of events taking

Table 3: Strength—ductility combination in high entropy alloys after RHP.

Composition	Phases present	Details of RHP (rolling type/annealing temperature/annealing time)	Yield strength (MPa)		Tensile strength (MPa)		Ductility (% elongation)		Product of tensile strength and ductility (PSD) (GPa × %)		Increase in PSD (%)	References
			Pre-TMP	Post-TMP	Pre-TMP	Post-TMP	Pre-TMP	Post-TMP	Pre-TMP	Post-TMP		
$Al_{0.25}CoCrFeNi$	FCC	RTR / 650 °C/ 48 h	173	470	428	879	79.3	48.23	33.94	42.39	24.9	50
$Al_{0.3}CoCrFeNi$	FCC	RTR /1050 °C/ 1440 min	207	204	335	588	40	69	13.40	40.57	202.8	51
$Al_{0.3}CoCrFeNi$	FCC	RTR /1050 °C/ 1440 min	207	204	335	588	40	69	13.40	40.57	202.8	51
$Al_{0.3}CoCrFeNi$	FCC	RTR / 1100 °C/1 h	175	188	325	553	60	95	19.50	52.54	169.4	51
$Al_{0.45}CoCrFeNi$	FCC	RTR / 1000 °C/1 h	298	667	591	923	30	30	17.73	27.69	56.2	52
$Al_{0.5}CoCrCuFeNi$	FCC + BCC	RTR /900 °C/ 300 min	578	612	884	750	10.7	28	9.46	21.00	122.0	43
$Al_{0.5}CoCrFeNi$	FCC + BCC	RTR /1200 °C /1 h	402	328	568	725	33.68	47.8	19.13	34.66	81.2	43
$Al_{0.6}CoCrFeNi$	FCC	RTR /1000 °C/ 1 h	561	795	750	1112	32	29.83	24.00	33.17	38.2	63
$AlCoCrFeNi_{2.1}$	$L1_2$ + B2	cryo-rolling/ 800 °C/ 1 h	615	1437	1105	1562	17	14	18.79	21.87	16.4	55
$AlCoCrFeNi_{2.1}$	$L1_2$ + B2	RTR / 700 °C/12 h	741	1110	1065	1340	7.5	11	7.99	14.74	84.5	65
$AlCoCrFeNi_{2.1}$	$L1_2$ + B2	warm rolling /1000 °C/1 h	510	705	1009	1194	17	31	17.15	37.01	115.8	68
$AlCoCrFeNi_{2.1}$	$L1_2$ + B2	RTR / 1100 °C/1 h	620	648	1050	1075	17	27	17.85	29.02	62.6	168
$Al_{3.37}$-$C_{0.69}$-$Co_{22.35}$-$Cr_{19.67}$-$Fe_{22.85}$-$Ni_{22.44}Mn_{8.62}$	FCC	RTR / 1000 °C/1 h	209	429	451	825	74	44	33.38	36.30	8.7	96
CrMnFeCoNi	FCC	RTR / 800 °C/1 h	210	700	463	930	57	54	26.39	50.22	90.3	70
FeCrCoMnNi	FCC	RTR / 650 °C /1 h	210	534	447	832	57	50	25.48	41.60	63.3	70
CrMnFeCoNi	FCC	RTR / 650 °C/1 h	210	625	463	855	57	51	26.39	43.60	65.2	140
CoCrFeMnNi	FCC	RTR /900 °C/ 1 h	168	328	346	670	43	52	14.88	34.84	134.1	140
CrMnFeCoNi	FCC	RTR / 920 °C/1 h	210	280	463	632	57	64	26.39	40.45	53.3	140
FeCoCrNiMn	FCC	RTR / 800 °C/1 h	195	378	491	700	70	54	34.37	37.80	10.0	79
$CoCrFeMnNiN_{0.01}$	FCC	RTR /900 °C/ 1 h	280	407	554	766	42	50	23.27	38.30	64.6	70
FeCoCrNiMn-0.5 at % C	FCC	RTR / 800 °C/1 h	262	517	572	790	50	40	28.60	31.60	10.5	79

Table 3: (continued)

Composition	Phases present	Details of RHP (rolling type/annealing temperature/annealing time)	Yield strength (MPa)		Tensile strength (MPa)		Ductility (% elongation)		Product of tensile strength and ductility (PSD) (GPa × %)		Increase in PSD (%)	References
			Pre-TMP	Post-TMP	Pre-TMP	Post-TMP	Pre-TMP	Post-TMP	Pre-TMP	Post-TMP		
FeCoCrNiMn-1 at % C	FCC	RTR / 800 °C/1 h	400	690	750	840	32	31	24.00	26.04	8.5	79
FeCoCrNiMn-1 at % C	FCC	RTR /1100 °C/ 30 min	400	380	750	810	32	74	24.00	59.94	149.8	79
FeCoCrNiMn-0.6 at % C	FCC	RTR / 900 °C/1 h	275	530	580	875	46.4	47	26.91	41.13	52.8	111
FeCoCrNiMn-2 at % C	FCC	RTR / 900 °C/6 h	446	581	723	857	15	33	10.85	28.28	160.6	49
$CoCrFeNi_{2.1}Nb_{0.2}$	FCC + Laves	cryo-rolling/800 °C/ 1 h	178	1219	598	1272	38.4	22	22.96	27.98	21.9	60
$Fe_{24}Co_{23}Ni_{24}Cr_{23}Ti_2Al_4$	FCC	RTR /1000 °C/ 2 h	293	709	418	861	22	17	9.19	14.64	59.3	45
$Fe_{40.4}Ni_{11.3}Mn_{34.8}Al_{7.5}Cr_6$												
- 1 at % C	FCC	Room temperature rolling (RTR) /1100 °C/4 h	355	405	734	914	46	46	33.76	42.04	24.5	99
$Fe_{41}Mn_{25}Ni_{24}Co_8Cr_2$	FCC	RTR / 800 °C/1 h	175	330	432	566	43	34	18.58	19.24	3.6	127
$Nb_{25}Ti_{25}Hf_{25}Zr_{25}$	FCC	RTR / 1000 °C/1 h	636	769	652	941	12	30	7.82	28.23	261.0	139

place (microstructural evolution) during annealing heat treatments, which depends on various parameters such as annealing temperature[56], annealing time[136], heating rate during annealing[45], etc. In this section, the role of various annealing parameters in microstructure evolution will be discussed in detail.

6.1 Annealing Temperature

The different mechanisms of microstructure evolution during heat treatments reported in literature are as follows: recovery[126,137], precipitation[138,139], recrystallization[140–142], grain growth[143–145], and annealing twins[146,147], etc. The mechanism in play triggering the microstructural change for HEA is dictated by annealing temperature[148]. The strong dependence on annealing temperature can be attributed to microstructural changes occurring, which in turn is strongly influenced by diffusion[149] which is exponentially related (Arrhenius dependence) to temperature[150]. Before annealing, rolling enhances the yield strength of FCC HEA manifold with considerable reduction in ductility[148]. Hence, the product of strength and ductility value reduced marginally, as shown in Fig. 8a[148]. However, annealing at different temperatures increases the PSD parameter significantly in comparison to both pre- and post-rolled HEA. Annealing renders higher yield strength values compared to pre-rolled status of HEA (Fig. 8a). The plausible reasons behind the enhanced mechanical properties post-annealing at different temperatures will be discussed vis-à-vis microstructural changes.

6.1.1 Recovery

The driving force for recovery during annealing post-deformation (static recovery) is the stored energy in the rolled specimens[151]. The static recovery in HEA involves steps such as dislocation interaction leading to formation of dislocation cells[68], reduction of dislocation density inside cell[152–154], intensification of texture[126], formation of subgrains[81], etc. The recovery temperature regime is dependent on compositional complexity and SFE of the material[155], etc. The higher is the SFE, more is the recovery as discussed earlier in hot rolling section. Static recovery is found to be dominant for FCC[72,98,137], BCC[81], and dual-phase[153,156] HEA after annealing below recrystallization temperature. The activation energy required for static recovery in conventional alloys is same as that of dislocation annihilation by climb and cross-slip, which is lower compared to that of recrystallization[157,158]. In terms of mechanical property evolution during recovery, the decrease in hardness of rolled FCC HEA is insignificant[72,148,156], whereas increase in ductility is notable[137]. The strength decrease during recovery was reported to be logarithmic and not as drastic as recrystallization[159]. This is the probable reason for increase in PSD after annealing below recrystallization temperatures of HEA (Fig. 8a).

6.1.2 Recrystallization

The mechanism of recrystallization involves the migration of HAGBs[105]. Hence, recrystallization needs higher thermal energy compared to recovery[157,158]. Above the recrystallization temperature, the recrystallization starts to dominate recovery. Similarly, the recrystallized fraction increased with increase in temperature in different HEA having various phases[62,72,81,160] possibly due to increase in HAGBs' mobility[161]. The HAGBs' mobility impeding elements such as carbon increase the recrystallization onset temperature[162]. The recrystallization activation energy in FCC HEA (549 kJ/mol)[163] is significantly higher compared to high manganese steel (230 kJ/mol)[164] and TWIP steel (229 kJ/mol)[165] due to precipitates pinning the grain boundaries in addition to solute drag effect. Hence, the nucleation of recrystallization in HEA requires higher annealing temperature compared to the conventional high-performance alloys. The recrystallization nucleation sources in HEA are deformation bands[52], grain boundaries[43], shear bands[98], second-phase particles[160], etc. The regions such as deformation bands, shear bands, etc. exhibited recrystallization initialization due to large driving force of stored energy[52,98]. The particle stimulated nucleation (PSN) is also prevalent in multiphase HEA. The harder phase deform less compared to softer phase and dislocation pile-up at the phase interface causes formation of deformation zone leading to nucleation of recrystallized grains[160]. The ductility is enhanced after recrystallization, and hence, the PSD value also gets enhanced with annealing for various HEA[140,166–169] which is shown in Fig. 8a[148].

6.1.3 Grain Growth Inhibition

As the HEA gets fully recrystallized, the grain growth starts dominating significantly at higher annealing temperatures compared to recrystallization temperature[152]. The excessive grain growth can deteriorate the strength of HEA[162]. The strategy of controlled precipitation in single-phase HEA is effectively employed in HEA to inhibit the excessive grain growth significantly[166]. The

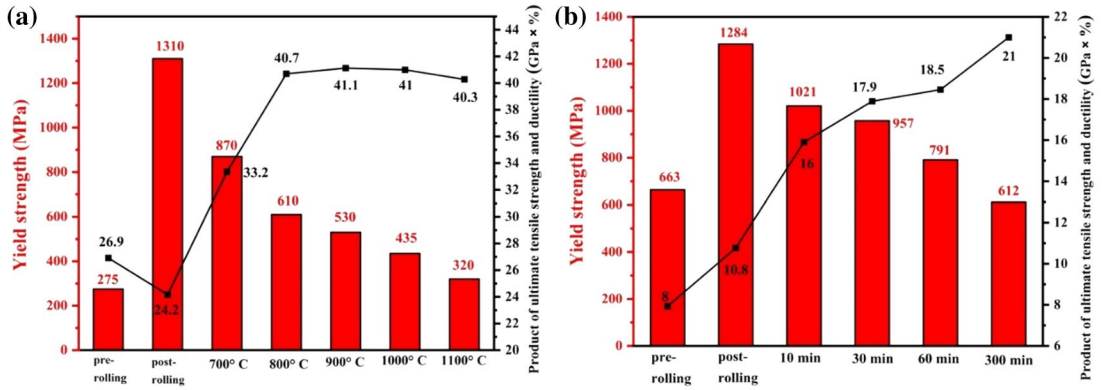

Figure 8: Enhancement in product of ultimate tensile strength and ductility (PSD in GPa × %) for high entropy alloys: **a** FeCoCrNiMn-0.6 at % carbon FCC alloy; annealed for 1 h at different temperatures[148]; **b** $Al_{0.5}$CoCrCuFeNi FCC alloy; annealed at 900 °C for various time[176].

calculation of phase diagrams (CALPHAD) is used as tool to optimally tune the precipitation depending on annealing temperatures[61,170]. This temperature has a significant role in deciding the size[67,171], distribution[167], and volume fraction of precipitates[139,172]. With increase in the annealing temperature, the coarsening of precipitates occurs by Oswald ripening mechanism[166]. Along with coarsening of precipitates, the volume fraction of precipitates reduces with increase in the annealing temperature[172]. Hence, annealing temperature plays a vital role in optimizing the precipitation and controlling grain growth thereof in single-phase HEA. Similar effect of grain boundary pinning is observed in multiphase alloys where harder phase inhibits the grain growth[35,166,173]. The volume fraction of harder second phase decreases with increase in annealing temperature. Hence, grain growth dominates with increasing annealing temperature[35,173]. In addition to this, the annealing twin fraction varies proportionally to grain size[143,146], and hence, annealing twinning increases as annealing temperature rises[142,173]. These microstructural changes result in higher activation energy for grain growth in HEA compared to the conventional alloys[163]. The yield strength and PSD are also higher than pre-rolling HEA even after annealing at temperatures significantly higher than recrystallization temperature (Fig. 8a). The excessive grain growth has been successfully inhibited with precipitates in single-phase HEA or with harder phase in multiphase alloys and the strength ductility synergy has been enhanced compared with pre-rolling HEA.

6.2 Annealing Time

After the microstructural evolution mechanism is ascertained by the annealing temperature, the microstructure can be tailored by varying the annealing time to enhance the PSD further[149,172,174,175]. The increasing trend in strength–ductility combination with increasing annealing time with respect to pre-rolled specimens was observed in $Al_{0.5}$CoCrCuFeNi HEA[176,177] (Fig. 8b). The specimens heat treated for different times exhibit higher yield strength values in comparison with pre-rolled HEA (Fig. 8b). The enhancement in the properties in relation to change in the microstructural features will be elaborated here.

The recrystallization kinetics in HEA is formulated with Johnson–Mehl–Avrami–Kolmogorov (JMAK) equation[160]. The recrystallization kinetics in HEA is slower[90] compared to other conventional high-performance alloys such as high manganese steel[164], TWIP steel[178], micro-alloyed steel[179] etc. The sluggish diffusion, severe lattice distortion effect and precipitates in HEA, results in delaying the recrystallization[6,90,163]. The sluggish diffusion renders restrictions on HAGBs' movement for recrystallization[90]. The severe lattice distortion leads to generation of local concentration fluctuation (LCF) regions which restricts the dislocation motion during the softening[90]. The precipitates formed during annealing in FCC HEA impede the mobility of HAGBs, and hence, the recrystallization requires higher thermal energy to occur[163].

The evolution of precipitates in HEA with increase in annealing time at particular temperature has been studied extensively[134,175]. The precipitate growth exponent (n) reported in various

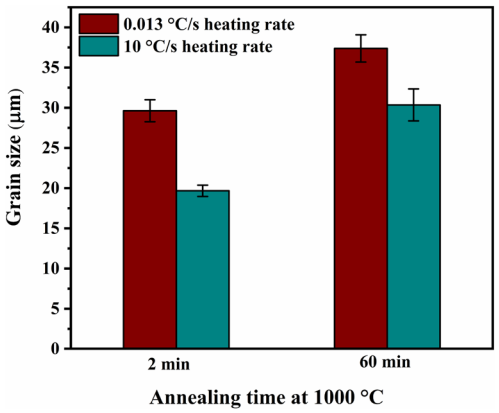

Figure 9: Significant finer grain size achieved in high heating rate sample compared with low heating rate samples after annealing at two different time at 1000 °C[45]

HEA is 3[148,169,180]. The significance of n = 3 lies in the fact that the coarsening of precipitates is via Oswald ripening mechanism[166] and volume diffusion[82,148]. The volume fraction of precipitates remains constant up to a specific annealing time and reduces drastically with further increase in the annealing time[172]. The grain boundary precipitates are stable, but the precipitates inside the grain start to dissolve in the matrix leading to overall decrease in volume fraction of precipitates[169].

The precipitates also slow down the kinetics of grain growth in FCC[136,169], BCC[81,145], and multiphase HEA[166,180]. The grain growth is described with modified Zener–Smith model (Z–S) model describing the pinning pressure exerted by the precipitates to restrict the grain growth[169]. Abnormal grain growth is also observed in FCC HEA due to heterogeneous distribution of precipitates in the initial stages of annealing[181]. Hence, the discussed microstructural evolution leads to achieving higher PSD values compared to pre-rolled HEA.

6.3 Heating Rate

The heating rate to reach annealing temperature also decides the microstructural evolution during annealing[182] and mechanical properties of conventional alloys[183]. The difference in grain size after annealing due to variation of heating rate in FCC HEA is represented in Fig. 9[45]. At high heating rates, HEA specimens exhibited lower grain size at two different annealing times than a lower heating rate (0.013 °C/s) of HEA specimens (Fig. 9). In lower heating rate specimens, the early nucleation and growth of recrystallized grains at preferred sites takes place[45,184]. Hence, larger grain size is achieved in low heating rate compared to high heating rate. This difference in final grain size leads to difference in the yield strength according to Hall–Petch relationship[162]. Hence, high heating rate achieves better yield strength and PSD compared to low heating rate[183].

6.4 Recrystallization Texture

The annealing of ternary medium entropy alloy leads to a strong cube recrystallization texture, similar to high SFE alloys. Quaternary and quinary medium entropy alloys retain some deformed texture components indicating delayed recovery phase[128]. Sluggish diffusion of grain boundaries in quaternary and quinary alloys hinders preferential texture growth, leading to randomisation of the texture. First-order annealing twins give rise to new annealing texture components such as *K* and *M* component apart from retained CR components[129]. No significant change in texture was observed with the annealing temperature. Bs, Goss, and S texture components appear post-cold rolling–annealing at 800 °C in CoCrFeMnNi (FCC) alloy with 1 atom % of carbon content elevating the strength[185]. Annealing twinning in Cantor alloy aids strong texture modification post-recrystallisation[126]. Randomisation of texture post-annealing was corroborated with Cellular Automata simulation results. Another study on annealing texture analysis of Cantor alloy showed S component dominant compared to brass and Goss components, and became stronger with annealing temperature[142].

Annealing of EHEA post-warm rolling at 800, 1000, and 1200 °C renders the FCC phase with retained deformed texture components. {112}<110> components are present post-annealing at 800 °C in B2 phase, and {111}<110> component shows up at 1200 °C[130]. {111}<110> component predominates along with ND fibre post-annealing of the HfZrTiTaNb HEA[131].

7 Severe Plastic Deformation

HEA have been processed and engineered using high-pressure torsion (HPT) to improve the strength, hardness, ductility, and superplasticity. The studies performed on HEA, out of which some significant cases will be discussed here. HPT combined with thermal annealing imparts 400% increase in hardness to $Al_{0.3}$CoCrFeNi HEA. Formation of ordered BCC phase at

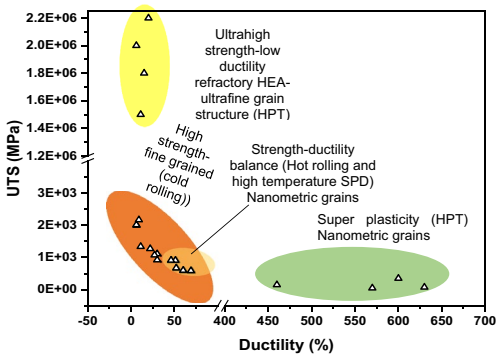

Figure 10: Ultimate tensile strength vs. ductility of SPD processed HEAs showing different properties post-HPT and rolling.

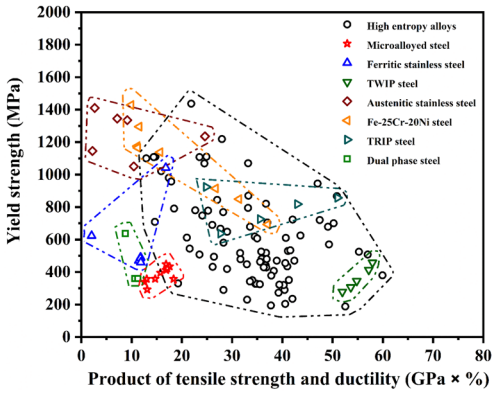

Figure 11: The comparison of post-rolling and annealing room-temperature tensile properties of high entropy alloys with other high performance.

high-temperature (500–700 °C) annealing as well as heterostructure promotes the elevation in hardness[186]. A grain size of 25 nm was achieved by HPT performed on $AlNbTiVZr_{0.5}$ alloy which had an initial coarse-grained structure with B2 matrix embedded with C14 Laves phase (rich in aluminium and Zirconium). Increase in nanohardness (550–665 HV) was observed in the B2 phase, whereas the C14 Laves phase becomes softer post-HPT[187]. Betterment in hardness in HPT processed HfNbTiZr BCC alloy from 2600 to 4450 MPa was realised by the aid of friction stress, possessing dislocation density of the order of 10^{16} m^{-2}[188]. Chromium oxide precipitates of size 7–10 nm in a matrix of CoCrFeMnNi alloy consisting of FCC + BCC solid solutions show hardness of 6700 MPa which is a staggering improvement in this kind of alloys[189]. Hardness improvement of 910 HV by forming a multiphase nanostructured microstructure obtained after long time (100 h) annealing of HPT processed Cantor alloy is reported by Schuh et al.[190]. Cyclic HPT (changes in strain path) creates unstable dislocation structure and fine grains which is responsible for high hardness of CoCuFeMnNi alloy[191]. Room temperature and cryo-HPT led to high hardness and fine grain morphology in Cantor alloy[192].

The synergy of tensile strength and ductility was demonstrated in case of HPT followed by annealing in $V_{10}Cr_{15}Mn_5Fe_{35}Co_{10}Ni_2$ alloy, possessing 1.54 GPa UTS and 6% of ductility[194]. $V_{10}Cr_{15}Mn_5Fe_{35}Co_{10}Ni_{25}$ alloy showcased a hardness of 505 MPa and tensile strength of 2 GPa with elongation failure of ~ 6%, post-HPT of coarse- and fine-grained starting material[195]. This was assisted by dislocation substructure formation along with twinning in the HEA. The Ashby plot for HPT processed and rolled HEAs is compared and shown in Fig. 10. The properties of fine and nanometer size grains post-HPT as well as rolling have been depicted in the plot. Nanometer size grain formation in HPT processed CoCrFeMnNi alloy improved the superplasticity behaviour (> 600% total elongation) at high temperatures; grain boundary sliding being instrumental for the former behaviour[198,199]. Addition of 2 atom % titanium in CoCrFeMnNi alloy followed by HPT showed 830% total elongation at 700 °C defining a new benchmark of superplasticity in HEA. This is possible due to grain size of 30 nm and retention of equiaxed nature of grains as titanium triggers sluggish diffusion[200].

8 Comparison of HEA Properties with High-Performance Materials Post-RHP

The comparison of tensile mechanical properties at room temperature of HEA with high-performance materials after RHP is presented in Fig. 10[201–209]. The best strength ductility combination (PSD) of RHPed HEA (maximum PSD of 60 GPa × % FeCoCrNiMn-1 at % C) is in the same range of TWIP steel (PSD: 58 GPa × %)[204], TRIP steel (PSD: 51 GPa × %)[208]. The highest yield strength (YS) values of RHPed HEA (maximum YS: 1437 MPa $AlCoCrFeNi_{2.1}$) are close to that of Fe-20 Cr-20 Ni steel (YS: 1428 MPa)[207], austenitic stainless steel (YS: 1410 MPa)[206], etc. The strength–ductility combination for many RHP HEA is also higher compared to microalloyed steel (PSD: 18.4 GPa × %)[201], dual-phase steel (PSD: 11.2 GPa × %)[209], and ferritic stainless steel (PSD: 16.8 GPa × %)[203] (Fig. 11). The microstructural evolution in the above-mentioned

alloys include precipitations inhibiting grain growth[203], twinning[204], grain refinement[207], etc. The role of various parameters during rolling and heat treatment processes is significant in these high-performance materials also in deciding final strength–ductility combination[201]. Figure 10 shows compilation of various yield strength and PSD values of the RHPed HEA and their comparison with conventional RHP high-performance materials[201]–[209].

9 Summary and Futuristic Approaches

In this review, the role of processing has been emphasized on room-temperature mechanical properties of a wide range of HEAs. The key variables of rolling and heat treatment process (RHP) that can be tuned to enhance the performance of synthesized HEA have been elaborated and debated. The strengthening mechanisms in HEA which operate during the deformation are explained in terms of metamorphosis of the microstructure. These changes are dependent on the nature of phases, working temperature along with SFE of the HEA. Tuning the total strain, strain path, and symmetricity of rolling optimally could impart additional strengthening. Further in the processing, the annealing temperature primarily dictates the microstructure evolution. The optimization of annealing time, heating rate, etc. enhances the strength–ductility synergy further. Following the evaluation of the role of possible parameters in influencing the microstructure evolution and room-temperature tensile properties during RHP in HEA, some futuristic ideas are enlisted below:

1. The strength–ductility combination can be enhanced to a desirable magnitude by combination of the advantages of multiple RHP domains in terms of temperature and, e.g., combination of cryo-rolling and warm rolling as well as asymmetric and symmetric rolling (hybrid rolling). This combination will enable the generation of hierarchical heterostructures with gradient microstructures which will help to promote the above-mentioned synergy.
2. Integrated Computational Materials Engineering (ICME) approach could find a solution for predicting processing–property correlation of HEA, by conducting lesser number of experiments. These simulation models can be used for better design of selective experiments to achieve optimal performance of HEA. The better design of experiments will promote energy efficiency and hassle-free methods to scale up the methods.
3. Microstructure and crystallographic texture simulation studies on HEA can be carried out to enable better maneuvering of microstructure–property correlation.
4. SPD techniques such as accumulative roll bonding can be performed to develop multilayers which inherently develop hierarchical microstructure (responsible for strength–ductility alliance) owing to the non-uniform strain-induced during the process. Along with developing the above properties and microstructures, the scale up of these processes is highly possible which could be undertaken to compete with the conventional materials in the market.

Publisher's Note

Acknowledgements

The authors are thankful to the online resources provided by Indian Institute of Technology, Madras in remote mode in the COVID-19 pandemic situation.

Declarations

Conflict of Interest

Authors declare that they have no potential conflict of interest.

Received: 12 November 2021 Accepted: 8 February 2022
Published: 24 March 2022

References

1. Murty BS, Yeh J-W, Ranganathan S, Bhattacharjee P (2019) High-entropy alloys. Elsevier, Amsterdam
2. Jien-Wei Y (2006) Recent progress in high entropy alloys. Ann Chim Sci Mat 31(6):633–648
3. Yeh JW, Chen YL, Lin SJ, Chen SK (2007) High-entropy alloys–a new era of exploitation. Trans Tech Publ, Materials Science Forum, pp 1–9
4. Cantor B (2014) Multicomponent and high entropy alloys. Entropy 16(9):4749–4768

5. Yeh J-W (2013) Alloy design strategies and future trends in high-entropy alloys. Jom 65(12):1759–1771
6. Tsai K-Y, Tsai M-H, Yeh J-W (2013) Sluggish diffusion in Co–Cr–Fe–Mn–Ni high-entropy alloys. Acta Mater 61(13):4887–4897
7. Ranganathan S (2003) Alloyed pleasures: multimetallic cocktails. Curr Sci 85(10):1404–1406
8. Raman L, Karthick G, Guruvidyathri K, Fabijanic D, Murty SN, Murty BS, Kottada RS (2020) Influence of processing route on the alloying behavior, microstructural evolution and thermal stability of CrMoNbTiW refractory high-entropy alloy. J Mater Res 35(12):1556–1571
9. Jalbuena A, Logier J, Nava J, Ravi V, Adil S, Murty BS (2018) Corrosion of High Entropy Alloys in Molten Salts, CORROSION 2018, NACE International
10. Fabijanic D, Bhattacharya R, Murty BS (2020) Enhancing the oxidation resistance of AlCrCoNiFe high entropy alloy by introducing nanocrystalline grain structure. In: International conference on nanostructured materials (NANO 2020), Engineers Australia, 2020, p 402
11. Miracle DB, Miller JD, Senkov ON, Woodward C, Uchic MD, Tiley J (2014) Exploration and development of high entropy alloys for structural applications. Entropy 16(1):494–525
12. Gludovatz B, Hohenwarter A, Catoor D, Chang EH, George EP, Ritchie RO (2014) A fracture-resistant high-entropy alloy for cryogenic applications. Science 345(6201):1153–1158
13. Yang L, Ge H, Zhang J, Xiong T, Jin Q, Zhou Y, Shao X, Zhang B, Zhu Z, Zheng S (2019) High He-ion irradiation resistance of CrMnFeCoNi high-entropy alloy revealed by comparison study with Ni and 304SS. J Mater Sci Technol 35(3):300–305
14. Edalati P, Floriano R, Mohammadi A, Li Y, Zepon G, Li H-W, Edalati K (2020) Reversible room temperature hydrogen storage in high-entropy alloy TiZrCrMnFeNi. Script Mater 178:387–390
15. Todai M, Nagase T, Hori T, Matsugaki A, Sekita A, Nakano T (2017) Novel TiNbTaZrMo high-entropy alloys for metallic biomaterials. Scripta Mater 129:65–68
16. He J, Wang H, Huang H, Xu X, Chen M, Wu Y, Liu X, Nieh T, An K, Lu Z (2016) A precipitation-hardened high-entropy alloy with outstanding tensile properties. Acta Mater 102:187–196
17. Karati A, Guruvidyathri K, Hariharan V, Murty BS (2019) Thermal stability of AlCoFeMnNi high-entropy alloy. Script Mater 162:465–467
18. Murty BS, Ranganathan S (1998) Novel materials synthesis by mechanical alloying/milling. Int Mater Rev 43(3):101–141
19. Varalakshmi S, Kamaraj M, Murty BS (2008) Synthesis and characterization of nanocrystalline AlFeTiCrZnCu high entropy solid solution by mechanical alloying. J Alloy Compd 460(1–2):253–257
20. Praveen S, Basu J, Kashyap S, Kottada RS (2016) Exceptional resistance to grain growth in nanocrystalline CoCrFeNi high entropy alloy at high homologous temperatures. J Alloy Compd 662:361–367
21. Vaidya M, Muralikrishna GM, Murty BS (2019) High-entropy alloys by mechanical alloying: a review. J Mater Res 34(5):664–686
22. Anupam A, Kottada RS, Kashyap S, Meghwal A, Murty BS, Berndt C, Ang A (2020) Understanding the microstructural evolution of high entropy alloy coatings manufactured by atmospheric plasma spray processing. Appl Surface Sci 505:144117
23. Vikram R, Murty BS, Fabijanic D, Suwas S (2020) Insights into micro-mechanical and texture response of additively manufactured eutectic high entropy alloy (AlCoCrFeNi2. 1). J Alloys Compounds 154034
24. Yao Y, Huang Z, Xie P, Lacey SD, Jacob RJ, Xie H, Chen F, Nie A, Pu T, Rehwoldt M (2018) Carbothermal shock synthesis of high-entropy-alloy nanoparticles. Science 359(6383):1489–1494
25. Van Den Avyle JA, Brooks JA, Powell AC (1998) Reducing defects in remelting processes for high-performance alloys. Jom 50(3):22–25
26. Miner R, Dreshfield R (1981) Effects of fine porosity on the fatigue behavior of a powder metallurgy superalloy. Metall Trans A 12(2):261
27. Gong H, Rafi K, Gu H, Ram GJ, Starr T, Stucker B (2015) Influence of defects on mechanical properties of Ti–6Al–4 V components produced by selective laser melting and electron beam melting. Mater Des 86:545–554
28. Chen L, Wei R, Tang K, Zhang J, Jiang F, He L, Sun J (2018) Heavy carbon alloyed FCC-structured high entropy alloy with excellent combination of strength and ductility. Mater Sci Eng A 716:150–156
29. Bahl S, Krishnamurthy AS, Suwas S, Chatterjee K (2017) Controlled nanoscale precipitation to enhance the mechanical and biological performances of a metastable β Ti-Nb-Sn alloy for orthopedic applications. Mater Des 126:226–237
30. Kalsar R, Ghosh P, Kundu S, Suwas S (2016) Effects of deformation texture and microstructure on recrystallization and grain growth in Twip steels. In: Proceedings of the 6th international conference on recrystallization and grain growth (ReX&GG 2016), Springer, New York, pp 137–145
31. Venkateswarlu K, Murty BS, Chakraborty M (2001) Effect of hot rolling and heat treatment of Al–5Ti–1B master alloy on the grain refining efficiency of aluminium. Mater Sci Eng A 301(2):180–186
32. Gurao N, Suwas S (2011) Texture evolution and operative mechanisms during large-strain deformation of nanocrystalline nickel. Philos Magn 91(5):798–817

33. Kusakin P, Belyakov A, Haase C, Kaibyshev R, Molodov DA (2014) Microstructure evolution and strengthening mechanisms of Fe–23Mn–0.3 C–1.5 Al TWIP steel during cold rolling. Mater Sci Eng A 617:52–60
34. An X, Wu S, Zhang Z, Figueiredo R, Gao N, Langdon T (2012) Enhanced strength–ductility synergy in nanostructured Cu and Cu–Al alloys processed by high-pressure torsion and subsequent annealing. Script Mater 66(5):227–230
35. Wani I, Sathiaraj GD, Ahmed M, Reddy S, Bhattacharjee PP (2016) Evolution of microstructure and texture during thermo-mechanical processing of a two phase Al0. 5CoCrFeMnNi high entropy alloy. Mater Char 118:417–424
36. Sathiaraj G, Bhattacharjee PP (2015) Effect of starting grain size on the evolution of microstructure and texture during thermo-mechanical processing of CoCrFeMnNi high entropy alloy. J Alloy Compd 647:82–96
37. Stepanov N, Tikhonovsky M, Yurchenko N, Zyabkin D, Klimova M, Zherebtsov S, Efimov A, Salishchev G (2015) Effect of cryo-deformation on structure and properties of CoCrFeNiMn high-entropy alloy. Intermetallics 59:8–17
38. Sathiaraj GD, Bhattacharjee PP (2015) Effect of cold-rolling strain on the evolution of annealing texture of equiatomic CoCrFeMnNi high entropy alloy. Mater Charact 109:189–197
39. Eleti RR, Bhattacharjee T, Zhao L, Bhattacharjee PP, Tsuji N (2018) Hot deformation behavior of CoCrFeMnNi FCC high entropy alloy. Mater Chem Phys 210:176–186
40. Zherebtsov S, Yurchenko N, Shaysultanov D, Tikhonovsky M, Salishchev G, Stepanov N (2020) Microstructure and mechanical properties evolution in HfNbTaTiZr refractory high-entropy alloy during cold rolling. Adv Eng Mater 2000105
41. Patel A, Wani I, Reddy S, Narayanaswamy S, Lozinko A, Saha R, Guo S, Bhattacharjee PP (2018) Strain-path controlled microstructure, texture and hardness evolution in cryo-deformed AlCoCrFeNi2. 1 eutectic high entropy alloy. Intermetallics 97:12–21
42. Han Z, Liang S, Yang J, Wei R, Zhang C (2018) A superior combination of strength–ductility in CoCrFeNiMn high-entropy alloy induced by asymmetric rolling and subsequent annealing treatment. Mater Charact 145:619–626
43. Guo T, Li J, Wang J, Wang WY, Liu Y, Luo X, Kou H, Beaugnon E (2018) Microstructure and properties of bulk Al0. 5CoCrFeNi high-entropy alloy by cold rolling and subsequent annealing. Mater Sci Eng A 729:141–148
44. Tsai C-W, Chen Y-L, Tsai M-H, Yeh J-W, Shun T-T, Chen S-K (2009) Deformation and annealing behaviors of high-entropy alloy Al0. 5CoCrCuFeNi. J Alloys Compounds 486(1–2):427–435
45. Sathiaraj G, Tsai C, Yeh J, Jahazi M, Bhattacharjee PP (2016) The effect of heating rate on microstructure and texture formation during annealing of heavily cold-rolled equiatomic CoCrFeMnNi high entropy alloy. J Alloy Compd 688:752–761
46. George EP, Curtin W, Tasan CC (2020) High entropy alloys: a focused review of mechanical properties and deformation mechanisms. Acta Mater 188:435–474
47. Diao H, Feng R, Dahmen K, Liaw P (2017) Fundamental deformation behavior in high-entropy alloys: an overview. Curr Opin Solid State Mater Sci 21(5):252–266
48. Hou J, Zhang M, Ma S, Liaw PK, Zhang Y, Qiao J (2017) Strengthening in Al0. 25CoCrFeNi high-entropy alloys by cold rolling. Mater Sci Eng A 707:593–601
49. Sunkari U, Reddy S, Rathod B, Kumar SS, Saha R, Chatterjee S, Bhattacharjee P (2020) Heterogeneous precipitation mediated heterogeneous nanostructure enhances strength–ductility synergy in severely cryo-rolled and annealed CoCrFeNi 2.1 Nb 0.2 high entropy alloy. Sci Rep 10(1):1–9.
50. He Y, Yang H, Zhao C, Zhang Y, Pan X, Li J, Wang J (2020) Enhancing mechanical properties of Al0. 25CoCrFeNi high-entropy alloy via cold rolling and subsequent annealing, J Alloys Compounds 154645
51. Li Z, Fu L, Peng J, Zheng H, Shan A (2020) Effect of annealing on microstructure and mechanical properties of an ultrafine-structured Al-containing FeCoCrNiMn high-entropy alloy produced by severe cold rolling. Mater Sci Eng A 139446
52. Hou J, Wang Z, Shi X, Wang Z, Qiao J, Wu Y () Strengthening of an Al 0.45 CoCrFeNi high-entropy alloy via in situ fabricated duplex-structured composites. J Mater Sci 1–16
53. Reddy S, Yoshida S, Bhattacharjee T, Sake N, Lozinko A, Guo S, Bhattacharjee P, Tsuji N (2019) Nanostructuring with structural-compositional dual heterogeneities enhances strength–ductility synergy in eutectic high entropy alloy. Sci Rep 9(1):1–9
54. Chen L, Cao T, Wei R, Tang K, Xin C, Jiang F, Sun J (2020) Gradient structure design to strengthen carbon interstitial Fe40Mn40Co10Cr10 high entropy alloys. Mater Sci Eng A 772:138661
55. Reddy S, Sunkari U, Lozinko A, Saha R, Guo S, Bhattacharjee P (2019) Microstructural design by severe warm-rolling for tuning mechanical properties of AlCoCrFeNi2. 1 eutectic high entropy alloy. Intermetallics 114:106601
56. Mehranpour MS, Shahmir H, Nili-ahmadabadi M (2020) Microstructure and excess free volume of severely cold shape rolled CoCrFeNiMn high entropy alloy. J Alloys Compounds 155672
57. Liu Y, Tu J, Tang Y, Zhu H, Huang C, Zhang Y-B, Tan L, Zhou Z-M (2020) Deformation substructural evolution

in transformation-induced plasticity high-entropy alloy during cold rolling. Mater Lett 127885
58. Wang M, Li Z, Raabe D (2018) In-situ SEM observation of phase transformation and twinning mechanisms in an interstitial high-entropy alloy. Acta Mater 147:236–246
59. Reddy T, Wani I, Bhattacharjee T, Reddy S, Saha R, Bhattacharjee PP (2017) Severe plastic deformation driven nanostructure and phase evolution in a Al0. 5CoCrFeMnNi dual phase high entropy alloy. Intermetallics 91:150–157
60. Sunkari U, Reddy S, Rathod B, Kumar D, Saha R, Chatterjee S, Bhattacharjee P (2020) Tuning nanostructure using thermo-mechanical processing for enhancing mechanical properties of complex intermetallic containing CoCrFeNi2. 1Nbx high entropy alloys. Mater Sci Eng A 769:138489
61. Stepanov N, Shaysultanov D, Chernichenko R, Ikornikov D, Sanin V, Zherebtsov S (2018) Mechanical properties of a new high entropy alloy with a duplex ultra-fine grained structure. Mater Sci Eng A 728:54–62
62. S. Zherebtsov, N. Yurchenko, E. Panina, A. Tojibaev, M. Tikhonovsky, G. Salishchev, N. Stepanov, Microband-induced plasticity in a Ti-rich high-entropy alloy. J Alloys Compds (2020) 155868.
63. Li Q, Zhang T, Qiao J, Ma S, Zhao D, Lu P, Wang Z (2020) Mechanical properties and deformation behavior of dual-phase Al0. 6CoCrFeNi high-entropy alloys with heterogeneous structure at room and cryogenic temperatures. J Alloys Compds 816:152663
64. Li Z, Tasan CC, Pradeep KG, Raabe D (2017) A TRIP-assisted dual-phase high-entropy alloy: grain size and phase fraction effects on deformation behavior. Acta Mater 131:323–335
65. Wani I, Bhattacharjee T, Sheikh S, Bhattacharjee PP, Guo S, Tsuji N (2016) Tailoring nanostructures and mechanical properties of AlCoCrFeNi2. 1 eutectic high entropy alloy using thermo-mechanical processing. Mater Sci Eng A 675:99–109
66. Singh A, Basha D, Matsushita Y, Tsuchiya K, Lu Z, Nieh T-G, Mukai T (2020) Domain structure and lattice effects in a severely plastically deformed CoCrFeMnNi high entropy alloy. J Alloys Compd 812:152028
67. Peng J, Li Z, Fu L, Ji X, Pang Z, Shan A (2019) Carbide precipitation strengthening in fine-grained carbon-doped FeCoCrNiMn high entropy alloy. J Alloy Compd 803:491–498
68. Zhou W, Fu L, Liu P, Xu X, Chen B, Zhu G, Wang X, Shan A, Chen M (2017) Deformation stimulated precipitation of a single-phase CoCrFeMnNi high entropy alloy. Intermetallics 85:90–97
69. Li L, Li Z (2020) Aging induced segregation and nano-precipitation in a severely deformed equiatomic high-entropy alloy. Mater Char 110369
70. Xiong F, Fu R, Li Y, Xu B, Qi X (2020) Influences of nitrogen alloying on microstructural evolution and tensile properties of CoCrFeMnNi high-entropy alloy treated by cold-rolling and subsequent annealing. Mater Sci Eng A 139472
71. Wu W, Guo L, Guo B, Liu Y, Song M (2019) Altered microstructural evolution and mechanical properties of CoCrFeNiMo0. 15 high-entropy alloy by cryogenic rolling. Mater Sci Eng A 759:574–582
72. Santos LA, Singh S, Rollett AD (2019) Microstructure and texture evolution during thermomechanical processing of Al 0.25 CoCrFeNi high-entropy alloy. Metall Mater Trans A 50(11):5433–5444
73. Su J, Raabe D, Li Z (2019) Hierarchical microstructure design to tune the mechanical behavior of an interstitial TRIP-TWIP high-entropy alloy. Acta Mater 163:40–54
74. Okamoto NL, Fujimoto S, Kambara Y, Kawamura M, Chen ZM, Matsunoshita H, Tanaka K, Inui H, George EP (2016) Size effect, critical resolved shear stress, stacking fault energy, and solid solution strengthening in the CrMnFeCoNi high-entropy alloy. Sci Rep 6:35863
75. Gwalani B, Gorsse S, Choudhuri D, Styles M, Zheng Y, Mishra RS, Banerjee R (2018) Modifying transformation pathways in high entropy alloys or complex concentrated alloys via thermo-mechanical processing. Acta Mater 153:169–185
76. Zhang Y, Tao N, Lu K (2009) Effect of stacking-fault energy on deformation twin thickness in Cu–Al alloys. Scripta Mater 60(4):211–213
77. Deng Y, Tasan CC, Pradeep KG, Springer H, Kostka A, Raabe D (2015) Design of a twinning-induced plasticity high entropy alloy. Acta Mater 94:124–133
78. Shen Y, Lu L, Lu Q, Jin Z, Lu K (2005) Tensile properties of copper with nano-scale twins. Scripta Mater 52(10):989–994
79. Guo L, Ou X, Ni S, Liu Y, Song M (2019) Effects of carbon on the microstructures and mechanical properties of FeCoCrNiMn high entropy alloys. Mater Sci Eng A 746:356–362
80. Moravcik I, Hadraba H, Li L, Dlouhy I, Raabe D, Li Z (2020) Yield strength increase of a CoCrNi medium entropy alloy by interstitial nitrogen doping at maintained ductility. Scripta Mater 178:391–397
81. Yurchenko NY, Panina E, Zherebtsov S, Tikhonovsky M, Salishchev G, Stepanov N (2019) Microstructure evolution of a novel low-density Ti–Cr–Nb–V refractory high entropy alloy during cold rolling and subsequent annealing. Mater Charact 158:109980
82. Senkov O, Pilchak A, Semiatin S (2018) Effect of cold deformation and annealing on the microstructure and tensile properties of a HfNbTaTiZr refractory high entropy alloy. Metall and Mater Trans A 49(7):2876–2892
83. Senkov O, Semiatin S (2015) Microstructure and properties of a refractory high-entropy alloy after cold working. J Alloy Compd 649:1110–1123

84. Wu W, Ni S, Liu Y, Song M (2016) Effects of cold rolling and subsequent annealing on the microstructure of a HfNbTaTiZr high-entropy alloy. J Mater Res 31(24):3815
85. Wang S, Wu M, Shu D, Sun B (2020) Kinking in a refractory TiZrHfNb07 medium-entropy alloy. Mater Lett 264:127369
86. Bertrand E, Castany P, Péron I, Gloriant T (2011) Twinning system selection in a metastable β-titanium alloy by Schmid factor analysis. Scripta Mater 64(12):1110–1113
87. Smallman RE, Bishop RJ (2013) Metals and materials: science, processes, applications. Elsevier, Amsterdam
88. Madhavan R, Ray R, Suwas S (2014) New insights into the development of microstructure and deformation texture in nickel–60 wt% cobalt alloy. Acta Material 78:222–235
89. Canova G, Kocks U, Stout M (1984) On the origin of shear bands in textured polycrystals. Scr Metall 18(5):437–442
90. Mohammad-Ebrahimi M, Zarei-Hanzaki A, Abedi H, Vakili S, Soundararajan C (2019) The enhanced static recrystallization kinetics of a non-equiatomic high entropy alloy through the reverse transformation of strain induced martensite. J Alloy Compd 806:1550–1563
91. Chen S, Oh HS, Gludovatz B, Kim SJ, Park ES, Zhang Z, Ritchie RO, Yu Q (2020) Real-time observations of TRIP-induced ultrahigh strain hardening in a dual-phase CrMnFeCoNi high-entropy alloy. Nat Commun 11(1):1–8
92. He F, Wang Z, Wu Q, Chen D, Yang T, Li J, Wang J, Liu C, Kai J-J (2018) Tuning the defects in face centered cubic high entropy alloy via temperature-dependent stacking fault energy. Scripta Mater 155:134–138
93. Sathiaraj GD, Bhattacharjee PP, Tsai C-W, Yeh J-W (2016) Effect of heavy cryo-rolling on the evolution of microstructure and texture during annealing of equiatomic CoCrFeMnNi high entropy alloy. Intermetallics 69:1–9
94. Rémy L, Pineau A, Thomas B (1978) Temperature dependence of stacking fault energy in close-packed metals and alloys. Mater Sci Eng 36(1):47–63
95. Zener C, Hollomon JH (1944) Effect of strain rate upon plastic flow of steel. J Appl Phys 15(1):22–32
96. Stepanov N, Shaysultanov D, Yurchenko N, Klimova M, Zherebtsov S, Salishchev G (2017) Microstructure Refinement in the CoCrFeNiMn High Entropy Alloy under Plastic Straining. Trans Tech Publ, Materials Science Forum, pp 1853–1858
97. Panigrahi SK, Jayaganthan R (2008) Effect of rolling temperature on microstructure and mechanical properties of 6063 Al alloy. Mater Sci Eng A 492(1–2):300–305
98. Fang W, Chang R, Liu B, Zhang X, Ji P, Qu X, Yin F (2018) Influence of warm-rolling and annealing temperature on the microstructure and mechanical properties of ductile non-equal molar Co40Cr-25Fe10Ni25 high entropy alloys. Mater Chem Phys 216:429–434
99. Wu M, Yang C, Kuijer M, Baker I (2019) Enhanced mechanical properties of carbon-doped FeNiMnAlCr high entropy alloy via hot-rolling. Mater Char 158:109983
100. Hassanpour-Esfahani M, Zarei-Hanzaki A, Abedi H, Kim H, Yim D (2019) The enhancement of transformation induced plasticity effect through preferentially oriented substructure development in a high entropy alloy. Intermetallics 109:145–156
101. Shafiee A, Nili-Ahmadabadi M, Kim HS, Jahazi M (2019) Development and microstructural characterization of a new wrought high entropy superalloy. Metal Mater Int 1–12
102. Shafiee A, Moon J, Kim HS, Jahazi M, Nili-Ahmadabadi M (2019) Precipitation behaviour and mechanical properties of a new wrought high entropy superalloy. Mater Sci Eng A 749:271–280
103. Sellars C, Whiteman J (1979) Recrystallization and grain growth in hot rolling. Metal Sci 13(3–4):187–194
104. Roy S, Suwas S (2013) Microstructure and texture evolution during sub-transus thermomechanical processing of Ti-6Al-4V-0.1 B alloy: Part I. Hot rolling in (α+β) phase field. Metall Mater Trans A 44(7):3303–3321
105. Humphreys FJ, Hatherly M (2012) Recrystallization and related annealing phenomena. Elsevier, Amsterdam
106. Brasche F, Wang J, Timokhina I, Haase C, Lapovok R, Molodov DA (2019) Mechanical twinning and texture evolution during asymmetric warm rolling of a high manganese steel. Mater Sci Eng A 764:138183
107. Elkatatny S, Gepreel MA, Hamada A, Nakamura K, Yamanaka K, Chiba A (2019) Effect of Al content and cold rolling on the microstructure and mechanical properties of Al5Cr12Fe35Mn28Ni20 high-entropy alloy. Mater Sci Eng A 759:380–390
108. Shabani A, Toroghinejad MR, Shafyei A, Cavaliere P (2018) Effect of cold-rolling on microstructure, texture and mechanical properties of an equiatomic FeCrCuMnNi high entropy alloy. Materialia 1:175–184
109. Biswas K, Gurao N (2016) Deciphering micro-mechanisms of plastic deformation in a novel single phase fcc-based MnFeCoNiCu high entropy alloy using crystallographic texture. Mater Sci Eng A 657:224–233
110. Gashti S, Fattah-Alhosseini A, Mazaheri Y, Keshavarz M (2016) Effects of grain size and dislocation density on strain hardening behavior of ultrafine grained AA1050 processed by accumulative roll bonding. J Alloy Compd 658:854–861
111. Klimova M, Stepanov N, Shaysultanov D, Chernichenko R, Yurchenko N, Sanin V, Zherebtsov S (2018) Microstructure and mechanical properties evolution of the Al, C-containing CoCrFeNiMn-type high-entropy alloy during cold rolling. Materials 11(1):53

112. Wang Z, Gao M, Ma S, Yang H, Wang Z, Ziomek-Moroz M, Qiao J (2015) Effect of cold rolling on the microstructure and mechanical properties of Al0. 25CoCrFe1. 25Ni1. 25 high-entropy alloy. Mater Sci Eng A 645:163–169
113. Gurao N, Sethuraman S, Suwas S (2013) Evolution of texture and microstructure in commercially pure titanium with change in strain path during rolling. Metall Mater Trans A 44(3):1497–1507
114. Gurao N, Sethuraman S, Suwas S (2011) Effect of strain path change on the evolution of texture and microstructure during rolling of copper and nickel. Mater Sci Eng A 528(25–26):7739–7750
115. Davenport S, Higginson RL, Sellars CM (1999) The effect of strain path on material behaviour during hot rolling of FCC metals. Philos Trans R Soc Lond Ser A: Math Phys Eng Sci 357(1756):1645–1661
116. Suwas S, Singh A (2003) Role of strain path change in texture development. Mater Sci Eng A 356(1–2):368–371
117. Reddy S, Ahmed M, Sathiaraj G, Bhattacharjee PP (2017) Effect of strain path on microstructure and texture formation in cold-rolled and annealed FCC equiatomic CoCrFeMnNi high entropy alloy. Intermetallics 87:94–103
118. Vikram R, Gaddam S, Kalsar R, Acharya S, Suwas S (2019) A fractal approach to predict the oxidation and corrosion behavior of a grain boundary engineered low SFE high entropy alloy. Materialia 7:100398
119. Ostafin M, Pospiech J, Schwarzer RA (2005) Microstructure and texture in copper sheets after reverse and cross rolling. Trans Tech Publ, Solid State Phenomena, pp 309–314
120. Shi P, Ren W, Zheng T, Ren Z, Hou X, Peng J, Hu P, Gao Y, Zhong Y, Liaw PK (2019) Enhanced strength–ductility synergy in ultrafine-grained eutectic high-entropy alloys by inheriting microstructural lamellae. Nat Commun 10(1):1–8
121. Ji Y, Park J (2009) Development of severe plastic deformation by various asymmetric rolling processes. Mater Sci Eng A 499(1–2):14–17
122. Verma KK, Suwas S, Kumar S (2020) Asymmetric Rolling of TZ73 Magnesium Alloy to Improve Its Ductility, Magnesium Technology. Springer 2020:189–196
123. Cui Q, Ohori K (2000) Grain refinement of high purity aluminium by asymmetric rolling. Mater Sci Technol 16(10):1095–1101
124. Sidor J, Miroux A, Petrov R, Kestens L (2008) Microstructural and crystallographic aspects of conventional and asymmetric rolling processes. Acta Mater 56(11):2495–2507
125. Beausir B, Biswas S, Kim DI, Tóth LS, Suwas S (2009) Analysis of microstructure and texture evolution in pure magnesium during symmetric and asymmetric rolling. Acta Mater 57(17):5061–5077
126. Haase C, Barrales-Mora LA (2018) Influence of deformation and annealing twinning on the microstructure and texture evolution of face-centered cubic high-entropy alloys. Acta Mater 150:88–103
127. Jeong H, Kim W (2018) Microstructures and mechanical properties of the non-equiatomic FeMnNiCoCr high entropy alloy processed by differential speed rolling. Mater Sci Eng A 727:38–42
128. Sathiaraj G, Ahmed M, Bhattacharjee PP (2016) Microstructure and texture of heavily cold-rolled and annealed fcc equiatomic medium to high entropy alloys. J Alloy Compd 664:109–119
129. Sathiaraj GD, Pukenas A, Skrotzki W (2020) Texture formation in face-centered cubic high-entropy alloys. J Alloys Compd 826:154183
130. Reddy SR, Sunkari U, Lozinko A, Guo S, Bhattacharjee PP (2019) Development and homogeneity of microstructure and texture in a lamellar AlCoCrFeNi 2.1 eutectic high-entropy alloy severely strained in the warm-deformation regime. J Mater Res 34(5):687–699
131. Eleti R, Raju V, Veerasham M, Reddy S, Bhattacharjee PP (2018) Influence of strain on the formation of cold-rolling and grain growth textures of an equiatomic HfZrTiTaNb refractory high entropy alloy. Mater Charact 136:286–292
132. Liu B, Xu L, Liu Y, Wang J, Wang J, Fang Q (2018) Effect of cold working and annealing on microstructure and properties of powder metallurgy high entropy alloy. Sci Chin Technol Sci 61(2):197–203
133. Wani I, Bhattacharjee T, Sheikh S, Lu Y, Chatterjee S, Bhattacharjee PP, Guo S, Tsuji N (2016) Ultrafine-grained AlCoCrFeNi2. 1 eutectic high-entropy alloy. Mater Res Lett 4(3):174–179
134. Huang Y-C, Tsao C-S, Lin C, Lai Y-C, Wu S-K, Chen C-H (2020) Evolution of Guinier-Preston zones in cold-rolled Al0. 2CoCrFeNi high-entropy alloy studied by synchrotron small-angle X-ray scattering. Mater Sci Eng A 769:138526
135. Li Q, Zhang T, Qiao J, Ma S, Zhao D, Lu P, Xu B, Wang Z (2019) Superior tensile properties of Al0. 3CoCrFeNi high entropy alloys with B2 precipitated phases at room and cryogenic temperatures. Mater Sci Eng A 767:138424
136. M. Klimova, D. Shaysultanov, R. Chernichenko, V. Sanin, S. Zherebtsov, N. Stepanov, Kinetics of recrystallization and grain growth in an ultra-fine grained CoCrFeNiMn-type high-entropy alloy, Journal of Physics: Conference Series, IOP Publishing, 2019, p. 012053.
137. Gangireddy S, Whitaker D, Mishra RS (2019) Significant contribution to strength enhancement from deformation twins in thermomechanically processed Al 0.1 CoCrFeNi microstructures. J Mater Eng Perform 28(3):1661–1667
138. Bała P, Górecki K, Bednarczyk W, Wątroba M, Lech S, Kawałko J (2020) Effect of high-temperature exposure

on the microstructure and mechanical properties of the Al5Ti5Co35Ni35Fe20 high-entropy alloy. J Mark Res 9(1):551–559

139. Ma Y, Wu S, Jia Y, Hu P, Bu Y, Chen X, Wang G, Liu J, Wang H, Zhai Q (2019) Hexagonal closed-packed precipitation enhancement in a NbTiHfZr refractory high-entropy alloy. Metals 9(5):485
140. Gu J, Ni S, Liu Y, Song M (2019) Regulating the strength and ductility of a cold rolled FeCrCoMnNi high-entropy alloy via annealing treatment. Mater Sci Eng A 755:289–294
141. Zaddach A, Scattergood R, Koch C (2015) Tensile properties of low-stacking fault energy high-entropy alloys. Mater Sci Eng A 636:373–378
142. Bhattacharjee P, Sathiaraj G, Zaid M, Gatti J, Lee C, Tsai C-W, Yeh J-W (2014) Microstructure and texture evolution during annealing of equiatomic CoCrFeMnNi high-entropy alloy. J Alloy Compd 587:544–552
143. Sathiaraj GD, Bhattacharjee PP (2015) Analysis of microstructure and microtexture during grain growth in low stacking fault energy equiatomic CoCrFeMnNi high entropy and Ni–60 wt% Co alloys. J Alloys Compounds 637:267–276
144. Sun S, Tian Y, Lin H, Dong X, Wang Y, Zhang Z, Zhang Z (2017) Enhanced strength and ductility of bulk CoCrFeMnNi high entropy alloy having fully recrystallized ultrafine-grained structure. Mater Des 133:122–127
145. Chen S, Tseng K-K, Tong Y, Li W, Tsai C-W, Yeh J-W, Liaw PK (2019) Grain growth and Hall-Petch relationship in a refractory HfNbTaZrTi high-entropy alloy. J Alloy Compd 795:19–26
146. Otto F, Hanold NL, George EP (2014) Microstructural evolution after thermomechanical processing in an equiatomic, single-phase CoCrFeMnNi high-entropy alloy with special focus on twin boundaries. Intermetallics 54:39–48
147. Sun S, Tian Y, Lin H, Yang H, Dong X, Wang Y, Zhang Z (2018) Transition of twinning behavior in CoCrFeMnNi high entropy alloy with grain refinement. Mater Sci Eng A 712:603–607
148. Klimova M, Shaysultanov D, Chernichenko R, Sanin V, Stepanov N, Zherebtsov S, Belyakov A (2019) Recrystallized microstructures and mechanical properties of a C-containing CoCrFeNiMn-type high-entropy alloy. Mater Sci Eng A 740:201–210
149. Zhang L, Fan J, Liu D, Zhang M, Yu P, Jing Q, Ma M, Liaw P, Li G, Liu R (2018) The microstructural evolution and hardness of the equiatomic CoCrCuFeNi high-entropy alloy in the semi-solid state. J Alloy Compd 745:75–83
150. Vaidya M, Pradeep K, Murty BS, Wilde G, Divinski S (2018) Bulk tracer diffusion in CoCrFeNi and CoCrFeMnNi high entropy alloys. Acta Mater 146:211–224
151. Martınez-de-Guerenu A, Arizti F, Gutiérrez I (2004) Recovery during annealing in a cold rolled low carbon steel. Part II: Modelling the kinetics. Acta Mater 52(12):3665–3670
152. Stepanov N, Shaysultanov D, Chernichenko R, Yurchenko NY, Zherebtsov S, Tikhonovsky M, Salishchev G (2017) Effect of thermomechanical processing on microstructure and mechanical properties of the carbon-containing CoCrFeNiMn high entropy alloy. J Alloy Compd 693:394–405
153. Xu Z, Li Z, Tong Y, Zhang W, Wu Z (2020) Microstructural and mechanical behavior of a CoCrFeNiCu4 non-equiatomic high entropy alloy. J Mater Sci Technol
154. Ma S, Qiao J, Wang Z, Yang H, Zhang Y (2015) Microstructural features and tensile behaviors of the Al0. 5CrCuFeNi2 high-entropy alloys by cold rolling and subsequent annealing. Mater Des 88:1057–1062
155. Wu Z, Bei H, Otto F, Pharr GM, George EP (2014) Recovery, recrystallization, grain growth and phase stability of a family of FCC-structured multi-component equiatomic solid solution alloys. Intermetallics 46:131–140
156. Hu X, Chen D (2018) Effect of ceramic rolling and annealing on mechanical properties of AlCoCrFeNi 2.1 eutectic high-entropy alloys. J Mater Eng Perform 27(7):3566–3573
157. Kuo C-M, Lin C-S (2007) Static recovery activation energy of pure copper at room temperature. Script Mater 57(8):667–670
158. Sf M, Je M (1996) Influence of alloying elements in solution on static recrystallization kinetics of hot deformed steels. ISIJ Int 36(8):1063–1069
159. Verlinden B, Driver J, Samajdar I, Doherty RD (2007) Thermo-mechanical processing of metallic materials. Elsevier, Amsterdam
160. Shabani A, Toroghinejad MR (2020) Evaluation of microstructure and texture formation during annealing of cold-rolled FeCrCuMnNi multiphase high-entropy alloy. Trans Nonferrous Metal Soc Chin 30(2):449–462
161. Huang Y, Humphreys F (1999) Measurements of grain boundary mobility during recrystallization of a single-phase aluminium alloy. Acta Mater 47(7):2259–2268
162. Wang Z, Baker I, Guo W, Poplawsky JD (2017) The effect of carbon on the microstructures, mechanical properties, and deformation mechanisms of thermomechanically treated Fe40. 4Ni11. 3Mn34. 8Al7. 5Cr6 high entropy alloys. Acta Mater 126:346–360
163. Annasamy M, Haghdadi N, Taylor A, Hodgson P, Fabijanic D (2019) Static recrystallization and grain growth behaviour of Al0. 3CoCrFeNi high entropy alloy. Mater Sci Eng A 754:282–294
164. Lü Y, Molodov DA, Gottstein G (2011) Recrystallization kinetics and microstructure evolution during annealing of a cold-rolled Fe–Mn–C alloy. Acta Mater 59(8):3229–3243
165. F. De las Cuevas, M. Reis, A. Ferraiuolo, G. Pratolongo, L.P. Karjalainen, V. García Navas, J. Gil Sevillano,

Kinetics of recrystallization and grain growth of cold rolled TWIP steel, Advanced Materials Research, Trans Tech Publ, 2010, pp. 153–158.
166. Hou J, Shi X, Qiao J, Zhang Y, Liaw PK, Wu Y (2019) Ultrafine-grained dual phase Al0. 45CoCrFeNi high-entropy alloys. Mater Des 180:107910
167. Stepanov N, Shaysultanov D, Klimova M, Sanin V, Zherebtsov S (2018) Strengthening of a CoCrFeNiMn-type high entropy alloy by regular arrays of nanoprecipitates. Trans Tech Publ, Materials Science Forum, pp 772–777
168. I. Wani, T. Bhattacharjee, S. Sheikh, Y. Lu, S. Chatterjee, S. Guo, P.P. Bhattacharjee, N. Tsuji, Effect of severe cold-rolling and annealing on microstructure and mechanical properties of AlCoCrFeNi2. 1 eutectic high entropy alloy, IOP Conference Series: Materials Science and Engineering, IOP Publishing, 2017, pp. 012018–1.
169. Yasuda HY, Miyamoto H, Cho K, Nagase T (2017) Formation of ultrafine-grained microstructure in Al0. 3CoCrFeNi high entropy alloys with grain boundary precipitates. Mater Lett 199:120–123
170. Cao B, Yang T, Liu W-H, Liu C (2019) Precipitation-hardened high-entropy alloys for high-temperature applications: a critical review. MRS Bull 44(11):854–859
171. Stepanov N, Yurchenko NY, Tikhonovsky M, Salishchev G (2016) Effect of carbon content and annealing on structure and hardness of the CoCrFeNiMn-based high entropy alloys. J Alloy Compd 687:59–71
172. Cho K, Fujioka Y, Nagase T, Yasuda HY (2018) Grain refinement of non-equiatomic Cr-rich CoCrFeMnNi high-entropy alloys through combination of cold rolling and precipitation of σ phase. Mater Sci Eng A 735:191–200
173. Reddy S, Sunkari U, Lozinko A, Guo S, Bhattacharjee P (2019) Microstructure and texture of a severely warm-rolled and annealed AlCoCrFeNi2. 1 eutectic high entropy alloy. J Phys Conf Ser IOP Publishing, p 012054
174. Chen S-T, Tang W-Y, Kuo Y-F, Chen S-Y, Tsau C-H, Shun T-T, Yeh J-W (2010) Microstructure and properties of age-hardenable AlxCrFe1. 5MnNi0. 5 alloys. Mater Sci Eng A 527(21–22):5818–5825
175. Huang Y-C, Tsao C-S, Wu S-K, Lin C, Chen C-H (2019) Nano-precipitates in severely deformed and low-temperature aged CoCrFeMnNi high-entropy alloy studied by synchrotron small-angle X-ray scattering. Intermetallics 105:146–152
176. Sheng HF, Peng LM (2014) Microstructure and tensile properties of Al0. 5CoCrCuFeNi high-entropy alloy. Appl Mech Mater Trans Tech Publ, pp 494–497
177. Tsai C-W, Tsai M-H, Tsai K-Y, Chang S-Y, Yeh J-W, Yeh A-C (2015) Microstructure and tensile properties of Al0. 5CoCrCuFeNi alloys produced by simple rolling and annealing. Mater Sci Technol 31(10):1178–1183
178. Bracke L, Verbeken K, Kestens L, Penning J (2009) Microstructure and texture evolution during cold rolling and annealing of a high Mn TWIP steel. Acta Mater 57(5):1512–1524
179. Mukunthan K, Hawbolt E (1996) Modeling recovery and recrystallization kinetics in cold-rolled Ti-Nb stabilized interstitial-free steel. Metall Mater Trans A 27(11):3410–3423
180. Yang H-X, Li J-S, Guo T, Wang W-Y, Kou H-C, Wang J (2020) Evolution of microstructure and hardness in a dual-phase Al 0.5 CoCrFeNi high-entropy alloy with different grain sizes. Rare Met 39(2):156–161
181. Zhang C, Zhu C, Shin S, Vecchio K (2018) Enhancement of< 001> recrystallization texture in non-equiatomic Fe-Ni-Co-Al-based high entropy alloys by combination of annealing and Cr addition. J Alloy Compd 768:277–286
182. Huang K, Marthinsen K (2015) The effect of heating rate on the softening behaviour of a deformed Al–Mn alloy with strong and weak concurrent precipitation. Mater Charact 110:215–221
183. Xu D, Li J, Meng Q, Liu Y, Li P (2014) Effect of heating rate on microstructure and mechanical properties of TRIP-aided multiphase steel. J Alloy Compd 614:94–101
184. Bampton C, Wert J, Mahoney M (1982) Heating rate effects on recrystallized grain size in two Al-Zn-Mg-Cu alloys. Metall Trans A 13(2):193–198
185. Li J, Gao B, Wang Y, Chen X, Xin Y, Tang S, Liu B, Liu Y, Song M (2019) Microstructures and mechanical properties of nano carbides reinforced CoCrFeMnNi high entropy alloys. J Alloy Compd 792:170–179
186. Tang Q, Huang Y, Huang Y, Liao X, Langdon T, Dai P (2015) Hardening of an Al0. 3CoCrFeNi high entropy alloy via high-pressure torsion and thermal annealing. Mater Lett 151:126–129
187. Stepanov N, Yurchenko NY, Gridneva A, Zherebtsov S, Ivanisenko YV, Salishchev G (2018) Structure and hardness of B2 ordered refractory AlNbTiVZr0.5 high entropy alloy after high-pressure torsion. Mater Sci Eng A 716:308–315
188. Gubicza J, Heczel A, Kawasaki M, Han J-K, Zhao Y, Xue Y, Huang S, Lábár JL (2019) Evolution of microstructure and hardness in Hf25Nb25Ti25Zr25 high-entropy alloy during high-pressure torsion. J Alloy Compd 788:318–328
189. Kilmametov A, Kulagin R, Mazilkin A, Seils S, Boll T, Heilmaier M, Hahn H (2019) High-pressure torsion driven mechanical alloying of CoCrFeMnNi high entropy alloy. Scripta Mater 158:29–33
190. Schuh B, Mendez-Martin F, Völker B, George EP, Clemens H, Pippan R, Hohenwarter A (2015) Mechanical properties, microstructure and thermal stability of a

nanocrystalline CoCrFeMnNi high-entropy alloy after severe plastic deformation. Acta Mater 96:258–268

191. Sonkusare R, Khandelwal N, Ghosh P, Biswas K, Gurao NP (2019) A comparative study on the evolution of microstructure and hardness during monotonic and cyclic high pressure torsion of CoCuFeMnNi high entropy alloy. J Mater Res 34(5):732–743
192. Podolskiy AV, Shapovalov YO, Tabachnikova ED, Tortika AS, Tikhonovsky MA, Joni B, Odor E, Ungar T, Maier S, Rentenberger C (2020) Anomalous evolution of strength and microstructure of high-entropy alloy CoCrFeNiMn after high-pressure torsion at 300 and 77 K. Adv Eng Mater 22(1):1900752
193. Praveen S, Bae JW, Asghari-Rad P, Park JM, Kim HS (2018) Ultra-high tensile strength nanocrystalline CoCrNi equi-atomic medium entropy alloy processed by high-pressure torsion. Mater Sci Eng A 735:394–397
194. Asghari-Rad P, Sathiyamoorthi P, Nguyen NT-C, Bae JW, Shahmir H, Kim HS (2020) Fine-tuning of mechanical properties in V10Cr15Mn5Fe35Co10Ni25 high-entropy alloy through high-pressure torsion and annealing. Mater Sci Eng A 771:138604
195. Asghari-Rad P, Sathiyamoorthi P, Bae JW, Shahmir H, Zargaran A, Kim HS (2020) Effect of initial grain size on deformation mechanism during high-pressure torsion in V10Cr15Mn5Fe35Co10Ni25 high-entropy alloy. Adv Eng Mater 22(1):1900587
196. Sathiyamoorthi P, Bae JW, Asghari-Rad P, Park JM, Kim JG, Kim HS (2018) Effect of annealing on microstructure and tensile behavior of CoCrNi medium entropy alloy processed by high-pressure torsion. Entropy 20(11):849
197. Wu W, Song M, Ni S, Wang J, Liu Y, Liu B, Liao X (2017) Dual mechanisms of grain refinement in a FeCoCrNi high-entropy alloy processed by high-pressure torsion. Sci Rep 7:46720
198. Shahmir H, He J, Lu Z, Kawasaki M, Langdon TG (2017) Evidence for superplasticity in a CoCrFeNiMn high-entropy alloy processed by high-pressure torsion. Mater Sci Eng A 685:342–348
199. Shahmir H, He J, Lu Z, Kawasaki M, Langdon TG (2016) Effect of annealing on mechanical properties of a nanocrystalline CoCrFeNiMn high-entropy alloy processed by high-pressure torsion. Mater Sci Eng A 676:294–303
200. Shahmir H, Nili-Ahmadabadi M, Shafiee A, Langdon TG (2018) Effect of a minor titanium addition on the superplastic properties of a CoCrFeNiMn high-entropy alloy processed by high-pressure torsion. Mater Sci Eng A 718:468–476
201. Zrnık J, Kvackaj T, Pongpaybul A, Sricharoenchai P, Vilk J, Vrchovinsky V (2001) Effect of thermomechanical processing on the microstructure and mechanical properties of Nb–Ti microalloyed steel. Mater Sci Eng A 319:321–325
202. Oñoro M, Macías-Delgado J, Auger M, de Castro V, Leguey T (2020) Mechanical properties and stability of precipitates of an ods steel after thermal cycling and aging. Nucl Mater Energy 100758
203. Lu H-H, Guo H-K, Liang W, Li J-C, Zhang G-W, Li T-T (2020) High-temperature Laves precipitation and its effects on recrystallisation behaviour and Lüders deformation in super ferritic stainless steels. Mater Des 188:108477
204. Gwon H, Kim JH, Kim J-K, Suh D-W, Kim S-J (2020) Role of grain size on deformation microstructures and stretch-flangeability of TWIP steel. Mater Sci Eng A 773:138861
205. Shakhova I, Dudko V, Belyakov A, Tsuzaki K, Kaibyshev R (2012) Effect of large strain cold rolling and subsequent annealing on microstructure and mechanical properties of an austenitic stainless steel. Mater Sci Eng A 545:176–186
206. Roy B, Kumar R, Das J (2015) Effect of cryorolling on the microstructure and tensile properties of bulk nano-austenitic stainless steel. Mater Sci Eng A 631:241–247
207. Xiong Y, He T, Li H, Lu Y, Ren F, Volinsky AA (2017) Annealing effects on microstructure and mechanical properties of cryorolled Fe-25Cr-20Ni steel. Mater Sci Eng A 703:68–75
208. Zhang B-G, Zhang X-M, Liu H-T (2020) Microstructural evolution and mechanical properties of Ni-containing light-weight medium-Mn TRIP steel processed by intercritical annealing. Mater Sci Eng A 139289
209. Gorain N, Walunj MG, Soni MK, Kumar BR (2020) Effect of continuous annealing process on various structure parameters of martensite of dual-phase steels. Arch Civ Mech Eng 20(1):1–10

Mr. Rushikesh Sabban is a research scholar in Indian Institute of Technology, Madras. He has obtained his MTech (Research) degree from Indian Institute of Science, Bangalore, where he worked in the laboratory of Prof. Satyam Suwas. He works in the area of high entropy alloys, 3D printing of Titanium alloys, and their thermomechanical processing. He has authored research papers and presented his work in conferences. He has been awarded the prestigious Prime Minister Research Fund to pursue Ph.D.

Dr. Khushbu Dash is a postdoctoral scholar in Indian Institute of Technology, Madras. She works with the group of Prof. B.S. Murty at IIT, Madras. She obtained her Ph.D. from the National Institute of Technology, Rourkela. She has worked with world renowned scientists in Charles University, Prague, and the University of Oxford. Her research interests span from metal matrix composites and their microstructural engineering to texture studies on severely plastically deformed metallic multilayers. She has authored many research papers published in prestigious journals. She has also been awarded national postdoctoral fellowship by SERB. She is a life member of EMSI.

Dr. Satyam Suwas is a professor and currently the Chair of Materials Engineering at Indian Institute of Science, Bangalore, India. He obtained his Ph.D. in Materials and Metallurgical Engineering from IIT Kanpur and worked at Defence Metallurgical Research Laboratory, Hyderabad; University of Lorraine, France; and RWTH Aachen, Germany, before joining Indian Institute of Science. His specialization includes materials processing, crystallographic texture, and mechanical behaviour of materials. He is the author of more than 300 research papers and has co-authored/co-edited three books. He is a Humboldt fellow and has also been conferred with the Friedrich Wilhelm Bessel Award by the Humboldt foundation, Germany. He was awarded Metallurgist of the year 2012 by Ministry of Steel, Govt. of India, and was conferred eminent engineering personality in the year 2014 by the Institution of Engineers, India, and G D Birla Gold Medal in 2020 by Indian Institute of Metals. He is a fellow of EMSI, INAE, and NASI.

Prof. B.S. Murty is the Director of IIT Hyderabad from August 26, 2019. He obtained his Ph.D. (1992) from IISc, Bangalore. He is an Institute Professor and Girija & R. Muralidharan Chair Professor at IIT Madras. He is also an Adjunct Professor at Ryerson University, Toronto, Canada, since 2011 and an associate faculty of school of engineering, University of British Columbia, Kelowna, Canada, since 2016. He has authored about 450 journal publications and 4 books. He has supervised 44 PhDs and 16 PhDs are ongoing. He has completed about 65 sponsored research projects and currently handling about 8 projects and filed 20 patents. He is a recipient of numerous awards including Shanti Swarup Bhatnagar Award (2007), JC Bose Fellowship award (2018-2023), Distinguished Alumnus Award of IISc Bangalore (2020), INAE Outstanding Teacher award (2019), Professor Extraordinarius from University of South Africa (2021), Honorary Doctorate from Deakin University, Australia (2017), Life time Achievement Award of IIT Madras (2016), GD Birla Gold Medal (2015), Eminent Materials Engineer Award (2011), Distinguished Alumnus Award of VNIT (2010), Metallurgist of the Year Award (2004), MRSI Medal (2004), INAE Young Engineer Award (1997), INSA Young Scientist Award (1995), Young Metallurgist Award (1994), and ISCA Young Scientists Award (1992). His is a fellow of TWAS, APAM, ASM, NAE, NA, NASc.